EUROPEAN JOURNAL OF REMOTE SENSING
2026, VOL. 59, NO. 1, 2650343
https://doi.org/10.1080/22797254.2026.2650343

Taylor & Francis by informa

RESEARCH ARTICLE

OPEN ACCESS Check for updates

Satellite-based analysis of maritime traffic effects on water quality indicators in the Mediterranean basin

Sofiia Drozd[a,b], Pavlo Henitsoi[a], Miquel Milian Ibáñez[c], Julen Guillermo Rostan Saez[c], Jose Alejandro Donate[c], Andrii Shelestov[a,b], Rodrigo Sedano[c] and Nataliia Kussul[a,b,d]

[a]Department of Mathematical Modeling and Data Analysis, Institute of Physics and Technology, National Technical University of Ukraine “Igor Sikorsky Kyiv Polytechnic Institute”, Kyiv, Ukraine; [b]Department of Space Information Systems and Technologies, Space Research Institute of National Academy of Sciences of Ukraine and State Space Agency of Ukraine, Kyiv, Ukraine; [c]Department of Computer Vision, ITCL Technology Center of Spain “Instituto Tecnológico de Castilla y León”, Burgos, Spain; [d]Department of Geographical Sciences, University of Maryland, College Park, MD, USA

ABSTRACT

This study investigates the impact of maritime traffic intensity on water quality indicators in the Mediterranean Sea during the post-pandemic period (2022–2024). We examined the relationships between the monthly vessel route density from EMODnet and satellite-derived indicators, including chlorophyll-a (Chl-a), suspended particulate matter (SPM), absorption by gelbstoff and detrital material (ADG), NO_2 and SO_2 (Sentinel-5P), as well as in-situ heavy-metal concentrations. Pearson correlations were computed across pixel, EEZ-IHO regional and basin-wide scales, and annual growth rates were estimated for traffic and environmental variables. To assess whether water-quality responses differ across traffic-intensity levels, we applied the Kruskal–Wallis test. The results show a strong positive temporal correlation between traffic intensity and NO_2 ($r = 0.83$, $p < 0.001$), whereas Chl-a ($r = -0.86$, $p < 0.001$), SPM and SO_2 display predominantly negative relationships. Passengers and fishing vessels exert the strongest effects, whereas cargo and tanker show weaker links. The Kruskal–Wallis test confirms that Chl-a and ADG distributions differ significantly across low-, medium-, and high-traffic areas. Among the heavy metals, Pb displays the most consistent positive spatial correlations. AGR analysis shows that declining traffic along major corridors coincides with reduced NO_2, whereas growth in the Adriatic corresponds to increased Chl-a and SPM.

ARTICLE HISTORY
Received 27 November 2025
Revised 10 March 2026
Accepted 19 March 2026

KEYWORDS
Water quality; marine traffic; vessel route density; satellite data; Pearson correlation; Kruskal–Wallis test

Introduction

Monitoring the quality of marine waters is a key prerequisite for ensuring the ecological stability and sustainable use of marine ecosystems. This is particularly relevant for the Mediterranean Sea, a semi-enclosed basin that connects Europe, Asia and Africa and serves as a vital hub of global trade, tourism and coastal urbanization. The region's high population density, intense maritime traffic, and limited water exchange with the Atlantic Ocean make it especially vulnerable to anthropogenic pressures and the accumulation of pollutants.

Recognizing these challenges, the European Union has launched several initiatives to enhance marine ecosystem protection and pollution monitoring. Among them is the iMERMAID project (Imermaidwebadm, 2025), which focuses on developing satellite—and artificial intelligence (AI)—approaches to monitor and mitigate chemical and anthropogenic pollution in the Mediterranean Sea, within whose framework of this study was conducted.

Among anthropogenic pressures, maritime traffic represents one of the most significant and continuously increasing sources of marine and atmospheric pollution in both coastal and open-sea environments (Selamoglu, 2021). Ship emissions, fuel combustion, oil spills, ballast water discharge and physical

CONTACT Sofiia Drozd sofi.drozd.13@gmail.com Department of Mathematical Modeling and Data Analysis, Institute of Physics and Technology, National Technical University of Ukraine “Igor Sikorsky Kyiv Polytechnic Institute”, 03056, 37, Beresteiskyi ave, Solomianskiy district, Kyiv, Ukraine

disturbances from vessel movement contribute to the accumulation of contaminants, including heavy metals and atmospheric aerosols, while also altering the biological, optical and chemical properties of seawater (Yuce & Altundag, 2020). Understanding how maritime traffic intensity influences marine environmental conditions is therefore essential for assessing the cumulative impact of human activities on ocean health.

A wide range of studies has investigated the effects of shipping activity on water quality in different marine regions. For example, Soon et al. (2021) analyzed pollution from insoluble particles and heavy metals associated with ship hull cleaning in Korean waters. Meanwhile, Ytreberg et al. (2021) developed a DAPSI(W)R(M)-based framework for evaluating ship emission impacts on marine ecosystems and air quality in the Baltic Sea, in which Drivers (D) are underlying forces, Activities (A) are human actions, Pressures (*P*) are environmental pressures, State (S) refers to environmental condition, Impacts on Welfare (I(W)) are effects on human well-being, and Responses as Measures (R(M)) are management actions. Ali et al. (2022) quantified toxic metal concentrations in shipbreaking. Similarly, Chen et al. (2024) modeled pollutant emissions from different vessel types under various navigation conditions in New York Harbor using the Ship Traffic Emission Assessment Model, version 2 (STEAM2), while Zhang et al. (2021) found that nitrogen oxides and sulfur dioxide emissions from vessels over the northwestern Pacific Ocean had measurable positive effects on phytoplankton growth. Morsy et al. (2022) assessed water quality in Port Said, Egypt, based on nutrient and contaminant concentrations, calculating multiple water quality indices (EI, TRIX and WQI) and measuring suspended solids, biochemical oxygen demand and heavy metals (Fe, Mn and Cu).

The COVID-19 pandemic provided a unique natural experiment for assessing how changes in maritime activity affect marine environments. Global shipping activity has declined sharply, leading to temporary improvements in air and water quality. Athul et al. (2024) reported reductions in global NO_2 pollution from shipping by 10%–30% during lockdowns, while Shi and Weng (2021) observed similar decreases in cargo ship emissions. In the Mediterranean, Braga et al. (2022) found reduced chlorophyll-a (Chl-a) concentrations in the Northern Adriatic Sea, and Saliba et al. (2021) identified a decline in SOx and NOx emissions. However, some studies showed that reduced vessel mobility did not always lower emissions (Mujal-Colilles et al., 2022), as many ships remained anchored or moored, maintaining pollution outputs. With post-pandemic economic recovery, maritime traffic has rebounded, raising new concerns about the resurgence of pollution levels.

Most of these previous studies, however, suffer from several limitations. They are often restricted to small coastal or port regions, rely heavily on in situ data from a limited number of stations, and focus on a single pollution type (e.g. heavy metals, NO_2 or oil spills). Consequently, they do not capture the high spatial and temporal variability of environmental conditions across the entire Mediterranean basin or account for interactions between atmospheric and marine pollutants.

Remote sensing offers a powerful alternative to overcome these limitations, providing continuous, multi-temporal coverage of key environmental indicators. He et al. (2021) used Landsat-8 data to analyze nutrient and chlorophyll patterns in the Yangtze River, while Drozd et al. (2025), Shelestov et al. (2024) and Yailymov et al. (2024) applied satellite data with machine learning to enhance the spatial resolution of Chl-a mapping in the Mediterranean. In the atmospheric domain, Yan et al. (2025) used Sentinel-5P to study SO_2, NO_2, and other air pollutants in China's coastal areas, linking them with vessel density. Baghdady and Abdelsalam (2024), Kussul et al. (2024) and Liubartseva et al. (2023) explored oil pollution detection and transport using Synthetic-aperture radar (SAR) and simulation models, demonstrating the capability of satellite-based monitoring for marine pollution assessment.

Despite these advances, comprehensive, basin-wide assessments integrating both marine and atmospheric indicators and analyzing their spatiotemporal relationships with maritime traffic remain scarce for the Mediterranean Sea. Moreover, the post-pandemic period (2022–2024), characterized by rapid traffic recovery and evolving environmental responses, has not yet been systematically investigated. Addressing these research gaps is crucial for understanding how human activity and environmental systems interact in the changing Mediterranean.

In this study, we address these gaps by conducting a multi-scale, basin-wide assessment of the interactions between maritime traffic intensity and marine environmental quality in the Mediterranean Sea during the post-COVID-19 period. Using harmonized multisource satellite and in-situ datasets, we jointly analyze key marine and atmospheric indicators, including chlorophyll-a (Chl-a), suspended particulate matter (SPM), absorption by gelbstoff and detrital material (ADG), heavy metals, NO_2, and SO_2, to quantify their spatial and temporal relationships with maritime traffic intensity.

Accordingly, our main objectives are as follows:

(1) To quantify spatial and temporal correlations between maritime route density and selected environmental indicators at multiple spatial scales (pixel, regional, and basin-wide).
(2) To analyze post-pandemic temporal trends in maritime activity and related environmental variables across the Mediterranean.
(3) To identify and map 'hotspot' areas where changes in water quality indicators correspond to increased traffic intensity, revealing regions most sensitive to shipping-related pressures.

Thus, the overall goal of this study is to provide a comprehensive, multi-scale assessment of the post-pandemic dynamics linking maritime traffic and environmental quality in the Mediterranean Sea. The findings contribute to the broader goals of the iMERMAID project, offering new insights and decision-support tools for sustainable marine management and pollution mitigation across one of the world's most environmentally stressed semi-enclosed seas.

Study area

The study area selected for this research is the Mediterranean Sea (International Hydrographic Organization (IHO) Sea Area, Figure 1), a semi-enclosed basin extending approximately 4,000 km from west to east and covering an area of about 2.5 million km^2, which corresponds to nearly 0.7% of the global ocean surface. It is located between Southern Europe, Northern Africa, and the Levantine region of Asia, making it one of the most strategically and economically important seas in the world. The Mediterranean connects to the Atlantic Ocean through the Strait of Gibraltar, to the Black Sea via the Turkish Straits, and to the Red Sea through the Suez Canal, making it a major hub of global maritime traffic.

The Mediterranean Sea is subdivided into four regional sub-basins (Figure 1), including the Western, Ionian and Central, Adriatic and Aegean-Levantine Seas, as well as into 30 exclusive economic zones (EEZs), which are maritime areas allocated to specific coastal states for the purpose of managing natural resources and economic activities. In addition, the International Hydrographic Organization (IHO) provides a standardized division of the Mediterranean into smaller hydrographic units to facilitate navigation, hydrographic surveying and maritime management. By combining the information on regional seas and national maritime boundaries, we can incorporate both environmental and managerial factors into our analysis. Figure 2 illustrates the intersection of EEZs and IHO hydrographic regions, resulting in

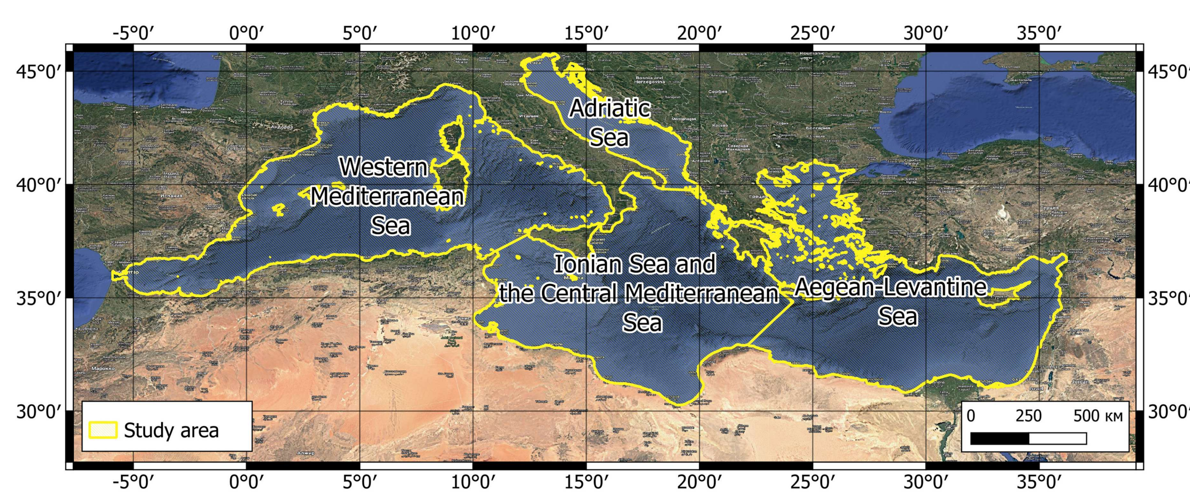

Figure 1. Study area.

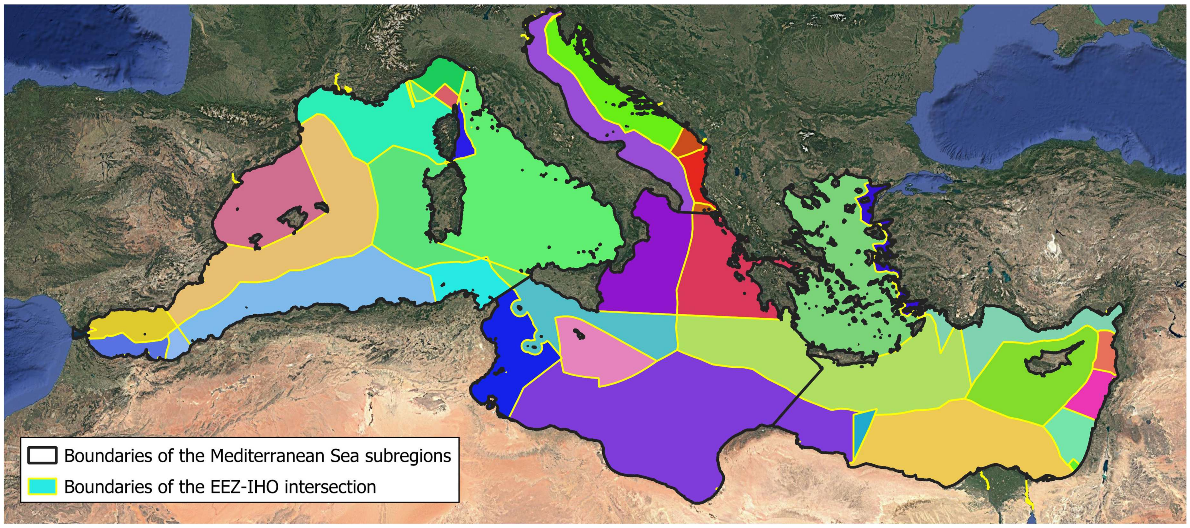

Figure 2. The intersection of the exclusive economic zones (EEZ) and IHO sea areas in the Mediterranean region.

47 subregions. The boundaries of this intersection were derived from the 'Marineregions: intersect of EEZs and IHO areas' dataset from the Marine Regions Geodatabase (Flanders Marine Institute, 2024) and will be used in our study.

The Mediterranean region contains more than 600 ports and terminals and is surrounded by 22 coastal states from three continents. This unique setting results in an exceptionally high density of human activities, including commercial shipping, fisheries and tourism. From a maritime perspective, the Mediterranean handles about 15% of global shipping activity by vessel calls and nearly 10% of global deadweight tonnage (Maritime transportation routes in the Mediterranean | GRID-Arendal, 2013). It accounts for 25% of the international seaborne trade and about 30% of global oil and gas maritime transport (UNEPMAP, 2021). Shipping is particularly concentrated in the Western Mediterranean, around the Strait of Gibraltar, and along the routes leading to the Suez Canal, which serve as critical chokepoints for international commerce.

Such intense economic activity has a measurable impact on the marine environment, particularly on water quality indicators. The studies show (Hourany et al., 2021), that high Chl-a concentrations have been observed mainly in the Adriatic Sea, the Gulf of Lion and parts of Aegean due to nutrient enrichment from river discharge and agricultural runoff.

Heavy metals tend to accumulate in eastern and southern Italy, Spain and Greece, largely as a result of shipping activity and industrial pollution (Ardila et al., 2024). Elevated acidification is most pronounced along busy shipping corridors, especially in the Adriatic Sea and in the Western Mediterranean, where emissions from vessel exhausts lower seawater pH (Lacoue-Labarthe et al., 2015). Additionally, oil spills, marine litter of anthropogenic origin and resuspension of sediments by ship propellers exacerbate the degradation of water quality, leading to elevated total suspended solids (TSS) and habitat stress for marine organisms.

Therefore, the Mediterranean Sea provides a dynamic and complex study area where natural conditions are strongly influenced by intense anthropogenic pressures, making it an ideal case for satellite-based monitoring of maritime traffic impacts on water quality indicators.

Data used

Maritime traffic intensity data

To assess maritime traffic intensity, we used the raster dataset 'EMSA Route Density Map', available through the European Marine Observation and Data Network (EMODnet) Map Viewer under the EMODnet Human Activities layers (EMODnet Map Viewer, 2025), an initiative funded by the European Commission.

These maps are generated by reconstructing ship routes based on recorded vessel positions, a method developed by the European Maritime Safety Agency (EMSA) and validated by EU Member States (European Marine Observation and Data Network, 2025). Each vessel trajectory is interpolated from positional records, and the resulting maps represent the number of reconstructed routes crossing each grid cell within a defined period of time. Thus, traffic density is expressed as the *cumulative count of vessel routes per pixel for a selected temporal resolution*.

The dataset provides a spatial resolution of 1 km and includes annual, seasonal and monthly traffic density layers starting from 2019, both for all vessel categories combined (Figure 3) and for specific vessel types such as cargo, tanker, passenger, fishing and others.

For this study, we extracted monthly data for the period 2022–2024 for each vessel type to assess their relative impact on water quality dynamics. The dataset was clipped to the boundaries of the Mediterranean Sea, producing 36 raster maps (one per month) for each of the five vessel categories and the composite category of all vessels, resulting in a total of 216 maps used for the analysis.

Water quality indicators

To evaluate the environmental impacts of maritime traffic in the Mediterranean Sea, we selected five key water quality indicators:

- Chlorophyll-a (Chl-a) concentration,
- Suspended particulate matter (SPM),
- Absorption due to gelbstoff and detrital material (ADG),
- Heavy metal concentration and
- Atmospheric pollutants (NO_2 and SO_2).

These parameters were chosen because they are widely recognized as sensitive indicators of anthropogenic pressures, particularly those associated with shipping activity, and they can be effectively monitored using satellite-based and ancillary datasets.

Chl-a (Chlorophyll-a) concentration

Chl-a concentration was included as a primary proxy for phytoplankton biomass and eutrophication. Maritime traffic contributes indirectly to nutrient enrichment through the atmospheric deposition of nitrogen compounds and wastewater discharges from vessels. Elevated Chl-a levels often indicate

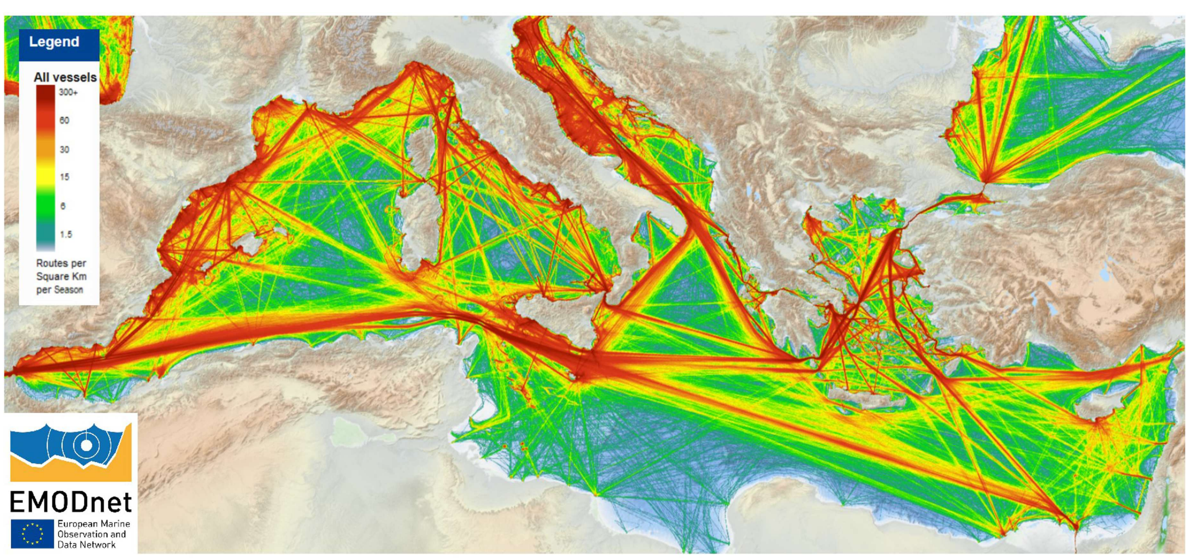

Figure 3. Monthly route density maps for all vessel types (2019–2025) from the EMODnet Map Viewer.

ecosystem stress and harmful algal blooms, which are relevant for assessing the ecological consequences of shipping.

Data on Chl-a concentration were obtained from the Japanese satellite JAXA GCOM-C using the dataset GCOM-C/SGLI L3 Chl-a concentration (V3) (Murakami, 2020), available on Google Earth Engine (GEE) and covering the period since December 2021. The dataset provides global coverage with a revisit time of 3–4 days and a spatial resolution of approximately 4638 m.

Although relatively coarse, previous studies have shown that GCOM-C Chl-a data correlate well with in-situ measurements in the Mediterranean region, in some cases outperforming higher-resolution sensors, such as Sentinel-3 (Drozd and Kussul, 2025; Yailymov et al., 2024). While satellite–in situ comparisons are inherently limited by scale differences, these studies indicate that GCOM-C reliably captures spatial gradients and temporal variability in Chl-a, providing a consistent, regularly updated dataset capable of representing regional patterns, which was the primary requirement for our study. Moreover, given the large spatial extent of the Mediterranean Sea, a coarser resolution was preferred to ensure computational feasibility when processing long time series. Using higher-resolution data (e.g. 300 m Sentinel-3), even a simple resampling step to align spatial resolution with vessel-route density would increase the pixel count by an order of magnitude, significantly affecting processing time and resource requirements. In addition, the GEE cloud environment, where the analysis was performed, does not provide other ready-to-use Chl-a products besides GCOM-C, and manually computing them could introduce errors and would be computationally prohibitive.

We downloaded and processed all available GCOM-C data for the period 2022–2024 within the GEE cloud environment, creating monthly composites. These composites were subsequently reprojected and resampled to a 1 km spatial resolution, ensuring consistency with the maritime traffic intensity dataset. As a result, we generated 36 Chl-a maps for the Mediterranean Sea, aligned with the temporal and spatial resolution of the vessel route density data, enabling direct comparison in the subsequent analysis (Figure 4).

Suspended particulate matter (SPM)

Suspended particulate matter (SPM) was included as a proxy for water turbidity and particulate load, which reflect riverine inputs, coastal resuspension and anthropogenic disturbance. Ship traffic can locally elevate SPM via propeller wash, wake-induced resuspension, and port operations, making it a relevant indicator for assessing potential traffic impacts on water clarity and benthic habitats.

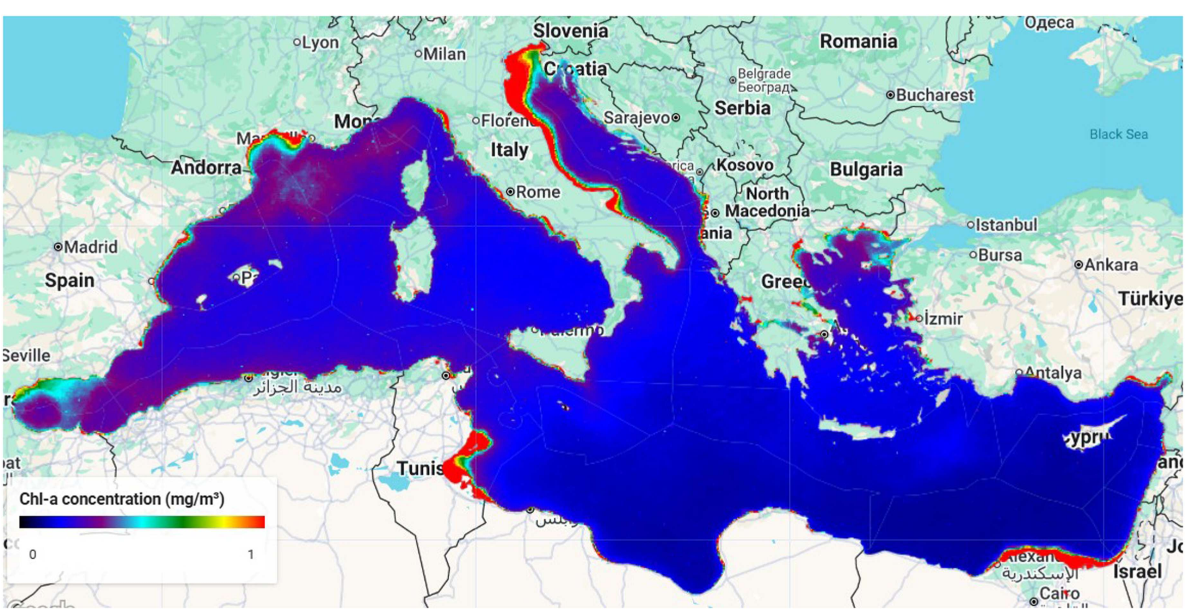

Figure 4. Mean concentrations of Chl-a over the Mediterranean Sea for the period 2022–2024.

We used the Copernicus Marine (CMEMS) Global Ocean Colour (Copernicus-GlobColour) Bio-Geo-Chemical, L4 monthly product. Specifically, we used 'Transparency, multi-sensor (4 km), monthly' dataset, which includes the variable 'Mass concentration of suspended matter in sea water' [g/m³] (Figure 5) (Copernicus Marine Environment Monitoring Service [CMEMS], 2025).

For this study, we analyzed monthly SPM values for 2022–2024 to align with traffic data. All rasters were clipped to the Mediterranean basin, reprojected and resampled to 1 km (bilinear) to match the EMODnet Route Density grid, and stacked into a monthly time series.

Absorption due to gelbstoff and detrital material (ADG)

We used the Mediterranean Sea Bio-Geo-Chemical L3 daily satellite observations (near real time) product as the main source of optical water-quality data. Specifically, we used the dataset Optics, multi-sensor (1 km) (cmems_obs-oc_med_bgc-optics_my_l3-multi-1km_P1D).

As a proxy for water-column optical clarity, we used the volume absorption coefficient of radiative flux in sea water due to dissolved organic matter and non-algal particles [m^{-1}], commonly referred to as ADG (absorption due to gelbstoff and detrital material). This parameter reflects the absorption of light by colored dissolved organic matter and detrital particles, which influences the transparency and color of the water column (Figure 6).

The data were derived from multiple satellite ocean color instruments and provided at a spatial resolution of approximately 1 km and a daily temporal resolution, with full coverage of the Mediterranean Sea.

Because the ADG product contains substantial spatial gaps at the native ~1 km resolution due to cloud cover and quality filtering, using only the available subset of pixels to generate annual composites would introduce spatial sampling bias, as the availability of cloud-free observations in the Mediterranean is geographically and seasonally structured. Therefore, the data were aggregated to a $0.1° \times 0.1°$ grid by assigning each pixel to its nearest grid cell through coordinate rounding. This aggregation increased the number of valid observations per analysis cell and allowed more stable annual ADG composites to be calculated (Geiger et al., 2021; Militino et al., 2019). The selection of the 0.1° resolution was supported by tests using aggregation windows of 0.05°, 0.1°, and 0.2°; among these, the 0.1° grid offered the optimal balance between spatial detail and stable sample sizes per cell.

To colocate ADG observations with maritime-traffic intensity, each valid ADG pixel was assigned to its corresponding 0.1° index cell. Candidate traffic records were then retrieved from expanding square neighborhoods of this index grid (3×3, 5×5, and 7×7 cells). As soon as a non-empty neighborhood was found, great circle distances were computed between the ADG pixel and all candidate traffic-cell centroids, and the density value of the nearest candidate was assigned to the pixel. Pixels for which no valid

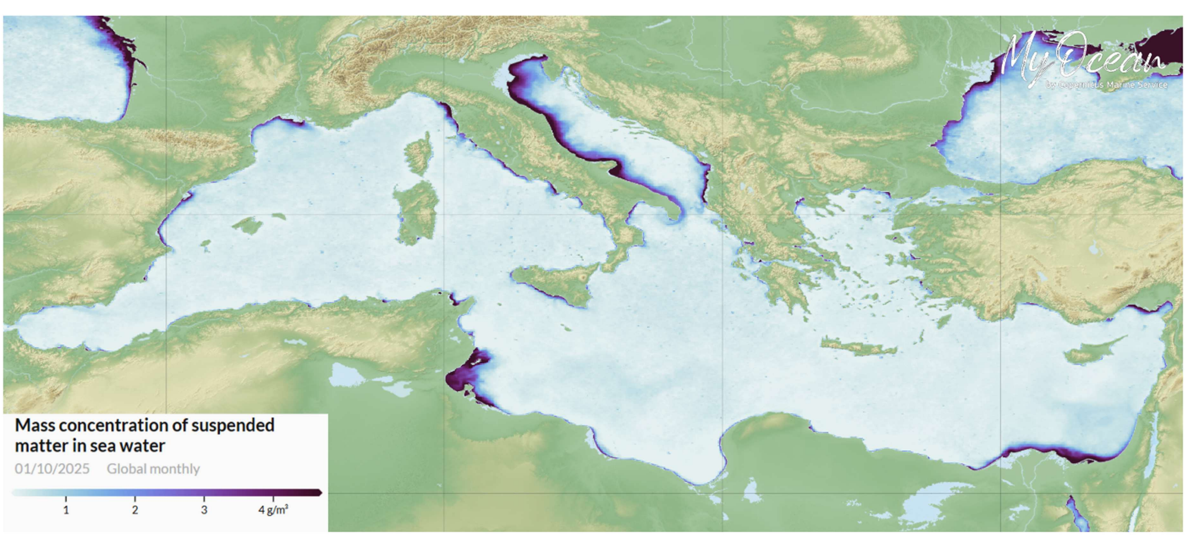

Figure 5. Map of SPM derived from Mediterranean Sea Bio-Geo-Chemical L3 satellite observations.

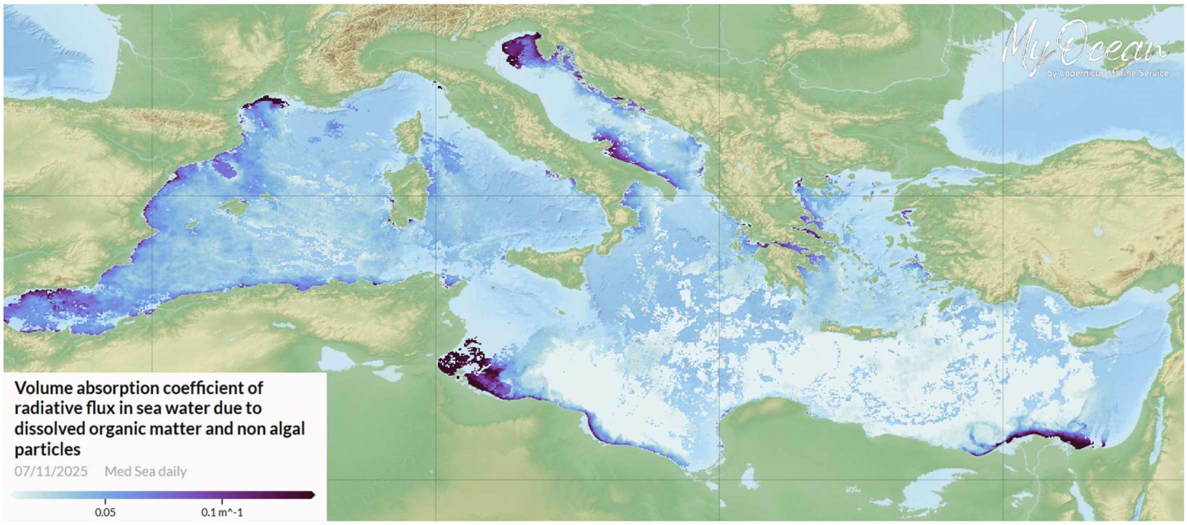

Figure 6. Map of ADG derived from Mediterranean Sea Bio-Geo-Chemical L3 satellite observations.

traffic cell was found within the 7×7 neighborhood were retained in the raw files but excluded from subsequent analyses.

Heavy metal concentration

Maritime shipping is recognized as one of the primary sources of heavy metal contamination in marine environments. Through fuel combustion, antifouling paints, cargo leakage and port activities, ships release trace metals that enter the water column and accumulate in sediments and marine organisms. Owing to their persistence, bioaccumulation and high toxicity, heavy metals are considered among the most hazardous environmental pollutants, posing long-term risks to marine ecosystems and human health.

In this study, we used data on the concentrations of four key heavy metals—cadmium (Cd), lead (Pb), mercury (Hg) and nickel (Ni)—from the dataset EMODnet Chemistry Contaminants: Metals and Metalloids (median values), version 2024 (EMODNET, 2025). This dataset provides spatially aggregated median concentrations of metals measured since 2012 across different environmental matrices (water, sediment and biota) within European regional seas, including the Mediterranean. The median concentration values are categorized into percentile ranges (0%–25%, 25%–75%, 75%–90% and >90%) and derived exclusively from validated measurements flagged as high-quality data (quality flags 1, 2 and 6, Q) according to the SeaDataNet quality flag schema.

The term water matrix refers to dissolved metal concentrations measured in surface seawater (0–15 m), representing the bioavailable fraction of contaminants. Sediment samples indicate long-term accumulation and reflect historical pollution trends. Biota refers to living marine organisms such as fish, mollusks and algae used as bioindicators to assess the biological uptake and trophic transfer of metals. Together, these matrices provide a comprehensive picture of the distribution, mobility and ecological risks of heavy metal contamination.

Sampling points in the Mediterranean Sea (Figures 7 and 8) are predominantly located along the European coastline, where monitoring networks are dense and where industrial and port activities are most extensive. From the EMODnet Chemistry database, we retrieved 3783 valid records (Table 1) covering the selected metals and matrices. These data were used to analyze spatial patterns of heavy metal concentrations and relate them to maritime traffic intensity and port proximity.

Atmospheric pollutants (NO_2 and SO_2)

In addition to direct water quality indicators, we also examined the concentrations of atmospheric gases such as nitrogen dioxide (NO_2) and sulfur dioxide (SO_2). These pollutants are among the

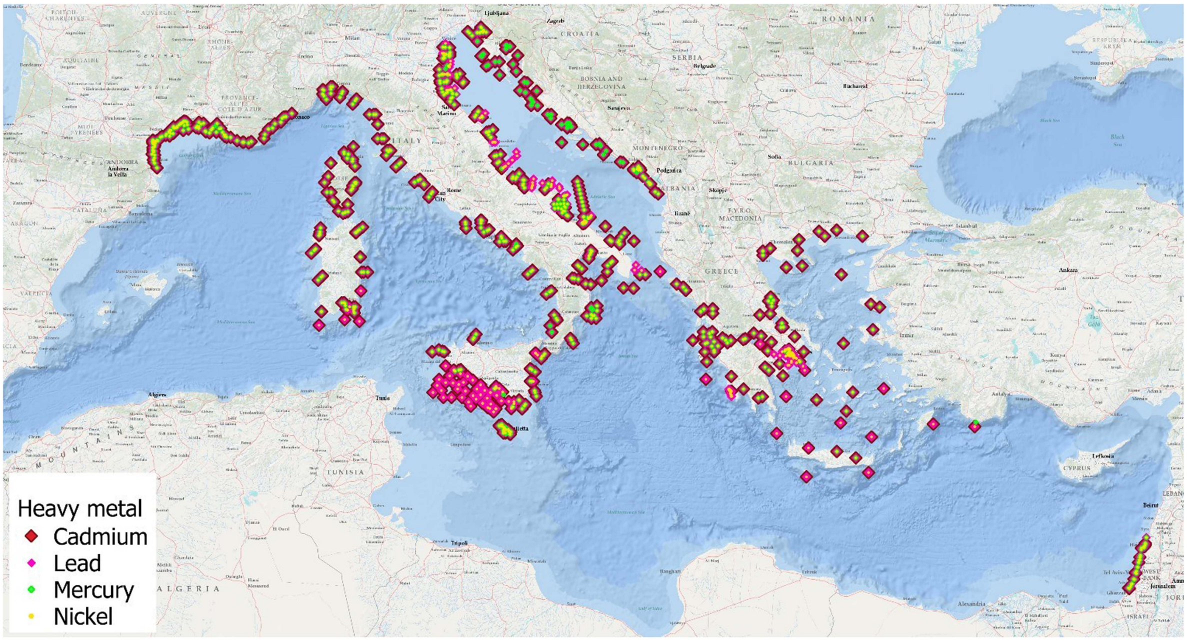

Figure 7. Spatial distribution of sampling stations measuring heavy metal concentrations in the Mediterranean Sea.

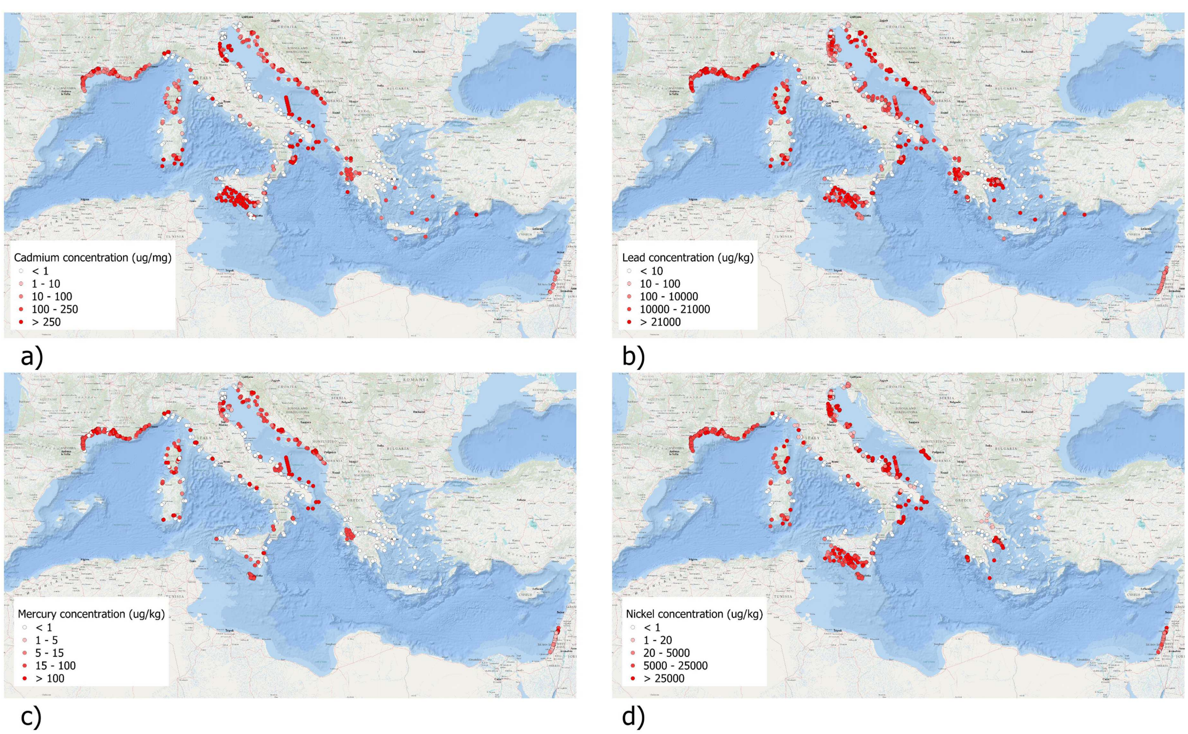

Figure 8. Distribution of median heavy metal concentrations: (a) cadmium (Cd), (b) lead (Pb), (c) mercury (Hg) and (d) nickel (Ni).

primary emissions from maritime transport and represent a growing environmental concern for both the marine and coastal atmosphere (Calgaro et al., 2025; Ledoux et al., 2021). Ship engines burning heavy fuel oil release large quantities of NO_x and SO_x compounds, which can subsequently undergo atmospheric reactions and deposit into the sea, contributing to acidification, nutrient enrichment and oxidative stress in marine ecosystems (Schlesinger, 2021; Wurtsbaugh et al., 2019). Monitoring these

Table 1. Number of heavy metal measurement samples, grouped by water matrix category.

Metal	Type	Sample count
Cadmium	Water	267
	Sediment	593
	Biota	50
	Total	**910**
Lead	Water	759
	Sediment	274
	Biota	50
	Total	**1083**
Mercury	Water	243
	Sediment	561
	Biota	91
	Total	**895**
Nickel	Water	243
	Sediment	561
	Biota	91
	Total	**895**

gases is therefore essential for understanding the indirect yet significant influence of maritime emissions on the marine environment.

To obtain data on NO_2 and SO_2 concentrations, we used satellite products from the Copernicus Sentinel-5P mission: NRTI NO_2: Near Real-Time Nitrogen Dioxide and NRTI SO_2: Near Real-Time Sulfur Dioxide (Copernicus Sentinel-5P [processed by ESA], 2018). These datasets provide vertical column density values near ground level, retrieved using the differential optical absorption spectroscopy (DOAS) technique. Both datasets offer a spatial resolution of approximately 0.01 arc degrees (~1.1 km) and are available on the Google Earth Engine (GEE) platform, covering the period from July 2018 to the present.

For this study, we collected all available Sentinel-5P NO_2 and SO_2 data from 2022 to 2024 (Figure 9) and generated monthly mean composites for each pollutant. These composites were reprojected and resampled to a 1 km spatial resolution to ensure consistency with the maritime traffic density dataset.

Methodology

Figure 10 presents the overall methodological framework used to assess the impact of maritime traffic on water quality in the Mediterranean Sea. To achieve this, we applied five complementary approaches:

(1) **Temporal correlation analysis**—to evaluate how variations in maritime traffic correspond to changes in water quality indicators over time at individual locations.
(2) **Spatial correlation analysis**—to measures how high or low traffic consistently co-occurs with high or low environmental indicator values across space at a given point in time.
(3) **Kruskal–Wallis test**—a nonparametric method used to test the hypothesis that different traffic levels (low, medium and high) are associated with statistically distinct distributions of selected indicators (specifically Chl-a and ADG), chosen due to the non-normal distribution of the data.
(4) **Temporal trend analysis**—to quantify long-term rates of change in maritime route density and water-quality indicators, highlight areas with increasing or decreasing trends, and evaluate how shifts in traffic intensity relate to simultaneous changes in environmental conditions.
(5) **Point-based spatial correlation**—to assess the spatial relationship between in-situ heavy-metal concentrations and maritime traffic intensity.

Correlation analysis

To assess the strength and nature of the relationships between maritime traffic intensity and water quality indicators, we conducted two types of correlation analysis using monthly datasets for the period 2022–2024: ***temporal correlation*** and ***spatial correlation***.

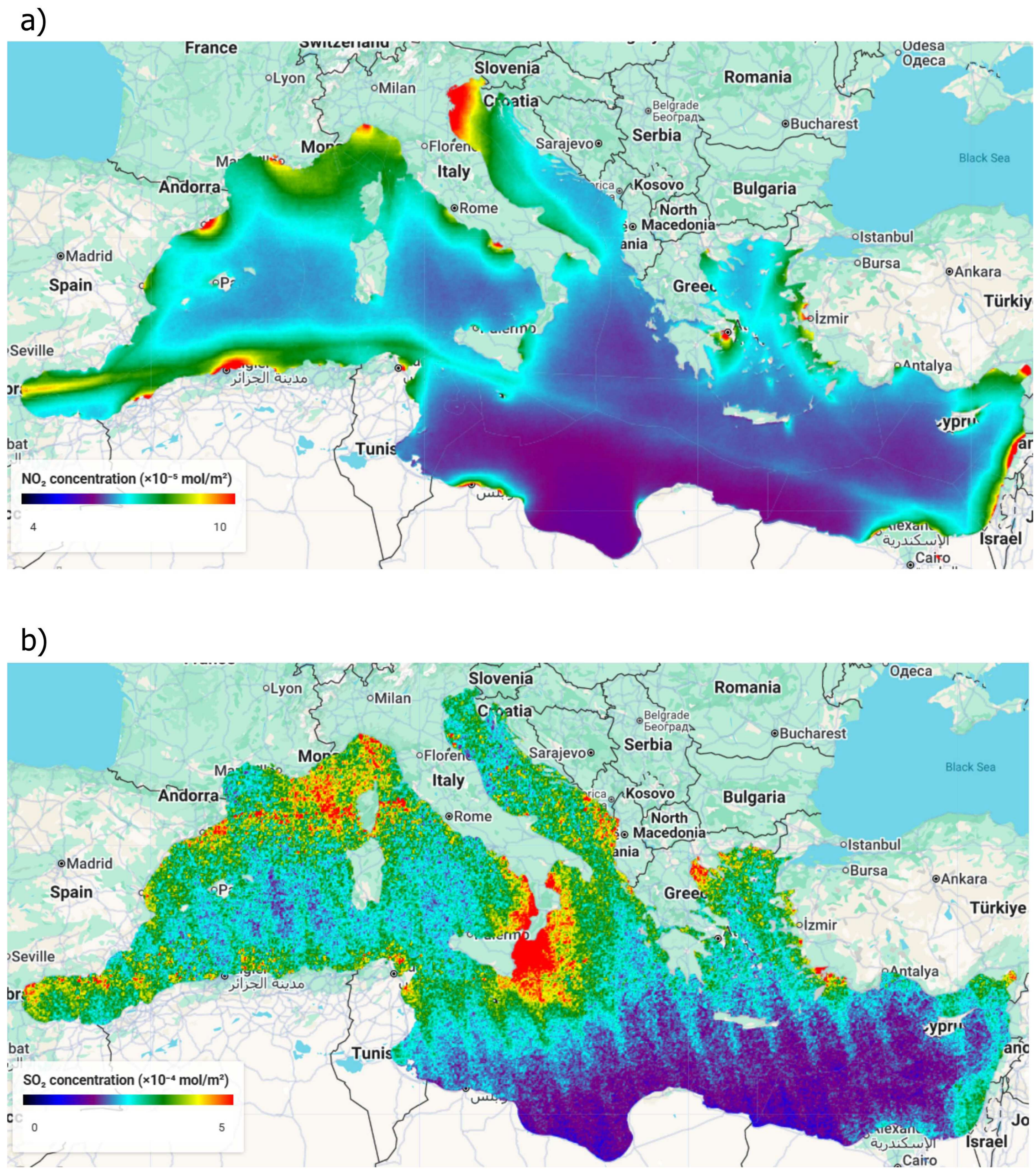

Figure 9. Mean concentrations of atmospheric pollutants over the Mediterranean Sea for the period 2022–2024: (a) nitrogen dioxide (NO_2) and (b) sulfur dioxide (SO_2).

These two perspectives answer different questions. Temporal correlation asks where changes in maritime traffic covary with changes in a water quality indicator over time at a given location, while spatial correlation asks where high or low values of traffic co-occur with high or low values of an indicator at a specific point in time.

Temporal correlation

Temporal correlation focuses on changes over time at fixed locations. For each location, we extracted monthly time series of maritime traffic density and the corresponding water quality indicator, and calculated the Pearson correlation coefficient between the two series (Figure 11).

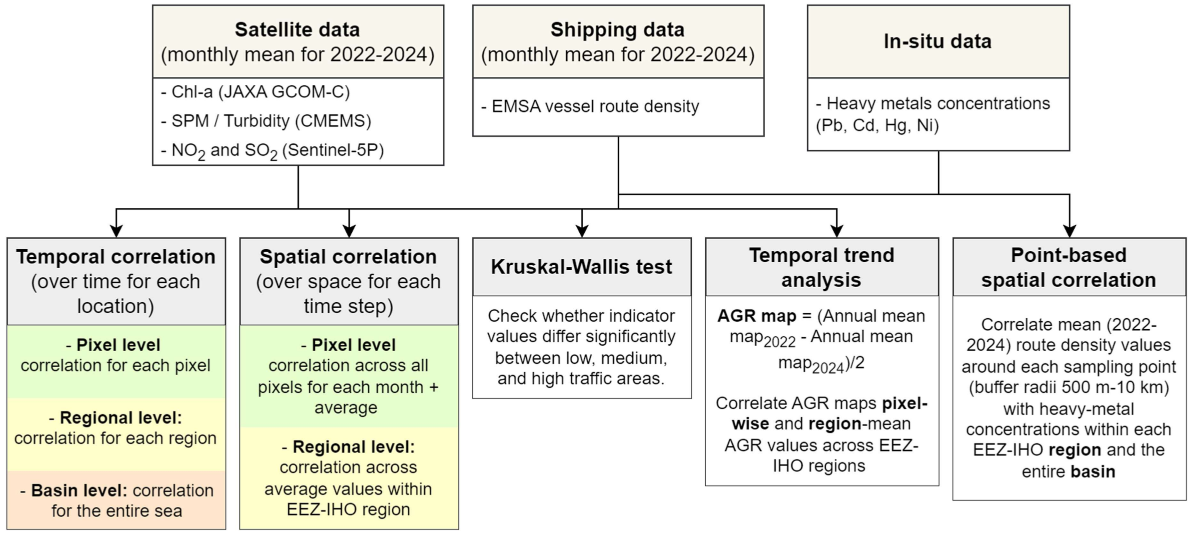

Figure 10. Proposed approaches for assessing the impact of maritime vessel route density on water quality.

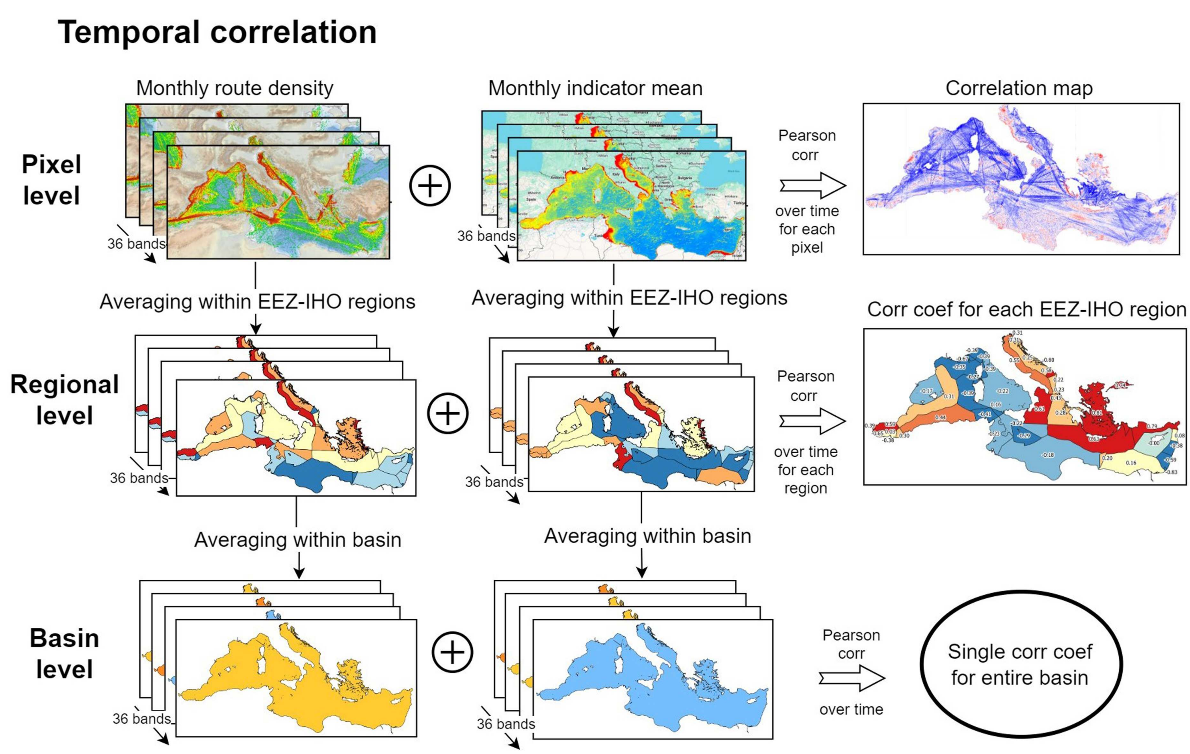

Figure 11. Workflow for temporal correlation analysis between vessel route density and environmental indicators.

The relationship between two time series was quantified using the Pearson correlation coefficient, defined as follows:

$$r_{temporal} = \sum_{i=1}^{n}((X_i - \bar{X}) * (Y_i - \bar{Y}))/(\sqrt{\sum_{i=1}^{n}(X_i - \bar{X})^2} * \sqrt{\sum_{i=1}^{n}(Y_i - \bar{Y})^2}), \quad (1)$$

where $r_{temporal}$ is the temporal Pearson correlation coefficient, X_i is the monthly mean maritime traffic density, Y_i is the corresponding monthly value of a water quality indicator, $\bar{X}$ and $\bar{Y}$ are the mean values of the respective time series and n is the number of temporal observations (months).

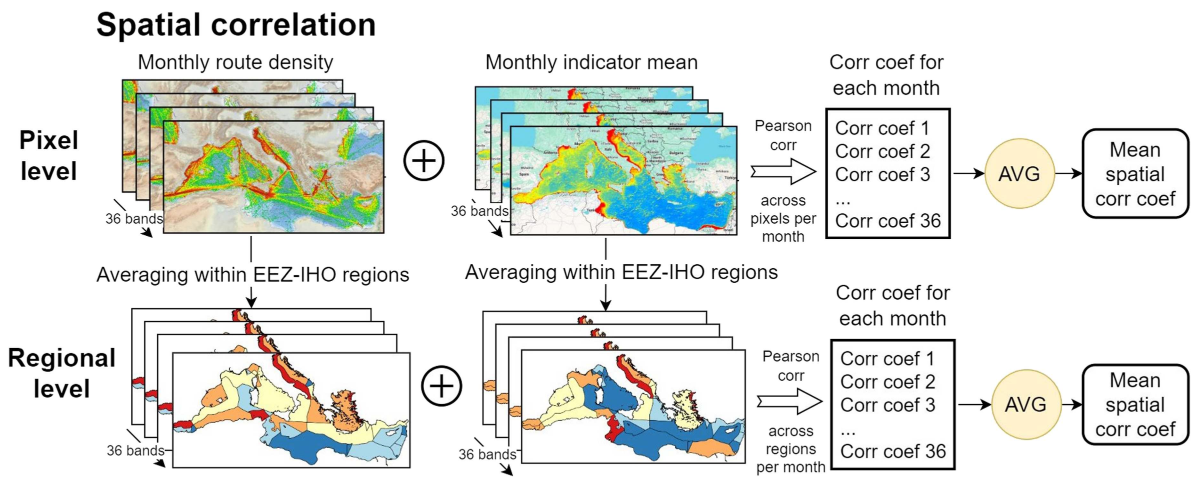

Figure 12. Workflow for spatial correlation analysis between vessel route density and environmental indicators.

The temporal correlation was calculated at three spatial levels:

(1) Pixel-level temporal correlation.

For each 1-km grid cell within the Mediterranean Sea, the Pearson correlation coefficient was computed between the monthly time series of maritime traffic density and each water quality indicator. This step allowed us to identify areas where traffic variations are closely followed by changes in environmental conditions.

(2) Regional-level temporal correlation.

To capture broader spatial trends, we first calculated the spatial median of the monthly route density and water quality indicators within each Mediterranean EEZ-IHO region (Figure 2). Then, we calculated the Pearson correlation coefficient between the resulting regional median time series of traffic intensity and the corresponding time series of each environmental indicator. This approach provides an integrated measure of how environmental conditions within a region respond to overall maritime activity.

(3) Basin-wide temporal correlation.

Finally, we averaged all pixel values across the entire Mediterranean basin for each month and applied Pearson's correlation to these basin-wide time series. This provided an overall measure of the statistical relationship between total maritime activity and general water quality conditions across the sea.

The regional and basin-wide averages were computed using the spatial averaging operator:

$$Z = 1/N * \sum_{j=1}^{N} Z_{j,t}, \tag{2}$$

where $Z_{j,t}$ is the value of the parameter in pixel j at time t and N is the total number of pixels within the corresponding region.

Spatial correlation

Spatial correlation examines the covariation between traffic intensity and environmental indicators across space at a given point in time. For each month, Pearson correlation coefficients were calculated using either all valid pixels across the Mediterranean basin or region-mean values within the EEZ-IHO regions (Formula 3, Figure 12). This procedure produced one correlation coefficient per each month, r_t.

$$r_t = \sum_{j=1}^{n} ((X_{j,t} - \overline{X_t}) * (Y_{j,t} - \overline{Y_t}))/(\sqrt{\sum_{j=1}^{n} (X_{j,t} - \overline{X_t})^2} * \sqrt{\sum_{j=1}^{n} (Y_{j,t} - \overline{Y_t})^2}), \tag{3}$$

where $X_{j,t}$ and $Y_{j,t}$ are the pixel values for maritime traffic density and a water quality indicator for month t, and $\overline{X_t}$ and $\overline{Y_t}$ are their spatial means across the domain.

Resulting monthly correlation values were then averaged to obtain the overall spatial correlation for the period 2022–2024:

$$r_{spatial} = \left(\sum_{t=1}^{n} r_t \right)/n. \tag{4}$$

Spatial correlation was calculated at two scales:

(1) **Pixel-based (Mediterranean-wide)**—correlation was calculated across all valid pixels in the Mediterranean basin.
(2) **Regional**—for each month, traffic values were first averaged within each EEZ-IHO region (Formula 2), so that regions served as spatial units instead of pixels. Correlations were then computed using these region-mean monthly values (Formula 3) and averaged over time (Formula 4). This allowed us to assess spatial relationships at a management-relevant scale and account for regional differences across the Mediterranean.

Point-based spatial correlation between vessel route density and heavy metal concentrations

Since heavy-metal samples were collected at discrete locations and not consistently collected over time, the temporal and raster-based spatial correlation methods applied to satellite indicators were not applicable. Therefore, to assess the spatial relationship between heavy-metal concentrations and maritime traffic, we used an approach specifically adapted for irregular, undated in-situ measurements.

First, we averaged the monthly vessel route density rasters over 2022–2024 to generate a long-term mean traffic map. Around each in-situ sampling point, we then created circular buffers at radii of 500 m, 1 km, 5 km and 10 km. Then, mean traffic intensity within each buffer was subsequently calculated as follows:

$$X_i = \frac{1}{k} \sum_{j=1}^{k} X_{mean(j)}, \tag{5}$$

where X_i is the average traffic assigned to point i, $X_{mean(j)}$ is the mean traffic value in pixel j and k is the number of pixels within the buffer.

For each heavy metal, buffer radius and sample matrix (all samples combined, sediment, biota and water), we computed Pearson correlation coefficients within each EEZ-IHO region separately (using Formula 3) to assess regional-scale relationships, as well as across the entire Mediterranean Sea to evaluate basin-wide associations.

In this way, we obtain correlation coefficients that capture how shipping-route density is associated with concentrations of each metal at multiple spatial distances from traffic routes, across three environmental matrices, and at two spatial scales—individual EEZ-IHO regions and the entire basin.

Kruskal–Wallis test

To evaluate how water-quality indicators respond to different levels of vessel route density, we applied the nonparametric Kruskal-Wallis H test. This test compares the distributions of a continuous variable across several independent groups without assuming normality and was selected specifically due to the non-Gaussian distribution of our data. In this study, the groups correspond to predefined vessel route density classes. We hypothesized that zones of high maritime traffic exhibit statistically distinct environmental distributions compared to low-traffic zones. To test the validity of this hypothesis, we focused the analysis on Chl-a and ADG as primary proxies susceptible to a broad range of shipping-related impacts, while for other indicators, we restricted the study to correlation-based methods.

The general procedure includes:

(1) reclassification of vessel route density data into intensity classes;
(2) ranking of indicator values across all samples;

(3) calculation of the H statistic and corresponding p value;
(4) interpretation of statistical significance and
(5) performing post-hoc pairwise comparisons (Dunn's test with Holm correction).

First, we reclassified the annual mean maritime route-density into three intensity classes using tertile cut points (33rd and 66th percentiles) computed on the pooled dataset (all years). We selected tertile-based thresholds because they ensure balanced sample sizes across classes and avoid patterns driven by extreme density values.

The resulting thresholds were 27 and 97 vessel routes/km^2, so observations were assigned as follows in Table 2.

Next, all mean annual Chl-a concentration and ADG values across all classes were pooled into one dataset and ranked from lowest to highest. Each observation received a rank R_j; identical values were assigned the average of their potential ranks. For each traffic class i, the mean rank was then calculated as follows:

$$\overline{R}_i = 1/n^i * \sum_{j}^{n^i} R_{ij}, \tag{6}$$

These mean ranks were used to compute the test statistic H according to Formula 7:

$$H = 12/((N(N+1))) \; * \; \sum_{i=1}^{k} n_i R_i^2 \; - \; 3 \; * \; (N+1), \tag{7}$$

where:

- k—number of maritime traffic classes,
- n_i—number of observations in class i,
- $\overline{R}_i$—mean rank of observations in class i,
- N—total number of observations.

The null hypothesis (H_0) states that all traffic intensity classes have the same median value of the studied indicator. Under H_0, the statistic H approximately follows a chi-square distribution with k−1 degrees of freedom. The p value was calculated as follows:

$$p = 1 - F_{\chi^2_{k-1}}(H), \tag{8}$$

where $F_{\chi^2_{k-1}}(H)$ is the cumulative chi-square distribution function.

If $p < 0.05$, we rejected the H_0 that all traffic-intensity classes share the same distribution, consistent with a reduction in the spatial contrast of water quality indicator values between high- and low-traffic areas.

When the Kruskal–Wallis test indicated statistically significant differences ($p < 0.05$), we performed post-hoc pairwise comparisons using Dunn's test. The test ranks all observations and compares the mean ranks between each pair of traffic-intensity classes (Low-Medium, Low-High and Medium-High) according to Formula 9:

$$Z_{ij} = ((\overline{R_i} - \overline{R_j}))/\sqrt{(N(N+1)/12 \; * \; (1/n_i + 1/n_j))}, \tag{9}$$

where $\overline{R}_i$ are the mean ranks in groups i and j, n_i and n_j are the sample sizes of each group and N is the total number of observations.

Table 2. Reclassification of maritime traffic density values into three intensity classes.

Class	Range of route density values	Description
Low	0–27	Low vessel density
Medium	28–97	Moderate vessel density
High	98–32,612	High vessel density

To control the family-wise error rate during multiple pairwise comparisons, we adjusted Dunn's p values using the Holm correction, which sequentially modifies the ordered p values. First, given m p values sorted from smallest to largest. Then, Holm-adjusted p values are computed as follows:

$$p_i^{adj} = \max_{j \le i}[(m - j + 1)p_j], \tag{10}$$

where p_i are the ordered raw p values and m is the number of comparisons.

A pairwise difference was considered statistically significant at $p_i^{adj} < 0.05$. This step ensures that the detected differences between classes are reliable and not due to chance.

Temporal trend analysis

To assess the dynamics and long-term tendencies of maritime traffic and water quality indicators in the Mediterranean Sea, we performed a temporal trend analysis for 2022–2024. This analysis quantified the direction and rate of change in both vessel route density and environmental parameters.

First, monthly data for each variable were aggregated into annual mean values. The absolute annual growth rate (AGR) for each indicator was then calculated as follows:

$$AGR = (X_{t2} - X_{t1})/(t2 - t1), \tag{11}$$

where X_{t1} and X_{t2} are the values at the beginning (2022) and end (2024) of the study period, respectively, and $(t2 - t1)$ is the number of years between them. Positive AGR values indicate an increasing trend, while negative values indicate a decrease. Larger absolute values reflect faster rates of change, whereas smaller values correspond to more stable conditions.

This procedure was first applied at the pixel level (Figure 13), producing basin-wide AGR maps for each variable. To characterize trends at a coarser spatial scale, AGR values from the pixel-based maps were then averaged within EEZ-IHO regions, yielding regional AGR estimates that reflect aggregated trends across each jurisdictional unit.

Finally, to examine the relationship between changes in maritime activity and environmental conditions, Pearson correlation coefficients were calculated between the AGR of maritime traffic intensity and those of each water quality indicator, both at pixel and regional scales. This analysis allowed identifying areas where increases in maritime traffic are most closely associated with corresponding changes in water quality, either indicating degradation or improvement.

In addition, within this step, we also calculated correlation coefficients among AGRs of the environmental parameters themselves to assess interdependencies and better understand how different pollution processes interact within the marine ecosystem.

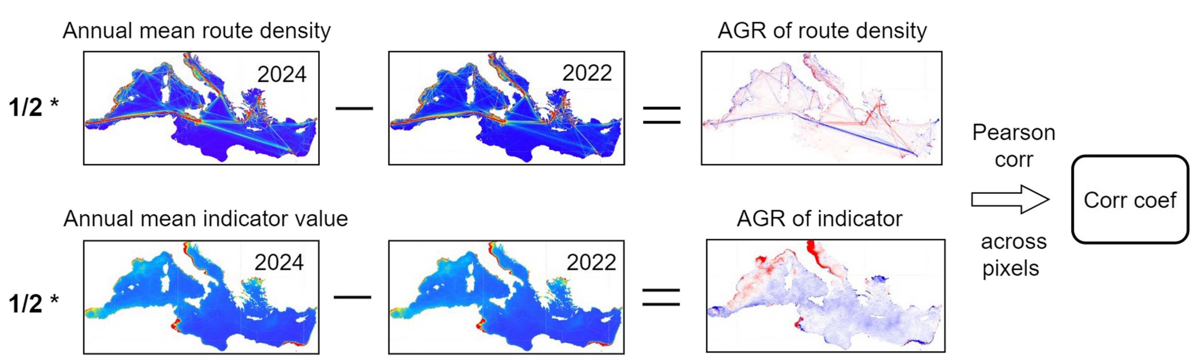

Figure 13. Workflow for calculating and correlating annual growth rates (AGR) of vessel route density and environmental indicators at the pixel level.

Results

Temporal correlation between maritime traffic and water quality indicators

Figures 14 and 15 present the temporal correlation patterns at the pixel and regional levels between maritime traffic density and key water quality indicators, including the Chl-a concentration, SPM, NO_2 and SO_2. Figure 16 illustrates scatterplots representing the correlation between these variables across the entire Mediterranean Sea.

At the pixel level (Figure 14), the correlation coefficients visually reproduce the main maritime routes for some indicators. A clear relationship is observed between route density and Chl-a (Figure 14a) as well as between route density and NO_2 (Figure 14c). Notably, the correlation with Chl-a is largely negative along the main shipping lanes (predominantly $r_{emporal} < -0.5$, $p < 0.001$), indicating that higher traffic corresponds to lower Chl-a concentrations. This pattern may reflect the influence of vessel movement and propeller-induced turbulence, which can enhance local mixing and temporarily disperse phytoplankton concentrations along frequently used routes. In contrast, NO_2 exhibits a strong positive correlation along these same routes ($r_{temporal} > 0.5$, $p < 0.001$), reflecting elevated atmospheric nitrogen dioxide associated with maritime emissions.

The temporal correlation between traffic density and SO_2 shows a similar pattern to that of Chl-a (Figure 14d), but it is generally weaker. Negative correlations are observed only along the western and northern shipping lanes, while no pronounced pattern is evident elsewhere. For SPM (Figure 14b), the pixel-level correlations reproduce shipping routes less clearly; only in the eastern basin is a positive correlation visible along the main traffic corridors.

When considering regionally averaged values (Figure 15), correlations vary significantly across Mediterranean economic subregions. For Chl-a (Figure 15a), a weak positive correlation is observed only in the Italian part of the Adriatic Sea ($r_{temporal} = 0.42$, $p < 0.01$), whereas in most other regions correlations are negative, particularly in the north-western basin ($r_{temporal} < -0.75$, $p < 0.001$).

In contrast, positive correlations between traffic density and NO_2 (Figure 15c) are observed across most of the basin and are strongest in regions with intense shipping activity, such as the Greek part of the Adriatic Sea ($r_{temporal} = 0.82$, $p < 0.001$), the Greek part of the Ionian Sea and the Italian part of the Tyrrhenian Sea ($r_{temporal} = 0.80$, $p < 0.001$), as well as across much of the western and central basin ($r_{temporal} > 0.75$, $p < 0.001$).

For regional temporal correlations involving SPM (Figure 15b) and SO_2 (Figure 15d), relationships are generally weaker and more heterogeneous. SPM shows predominantly negative correlations, particularly in

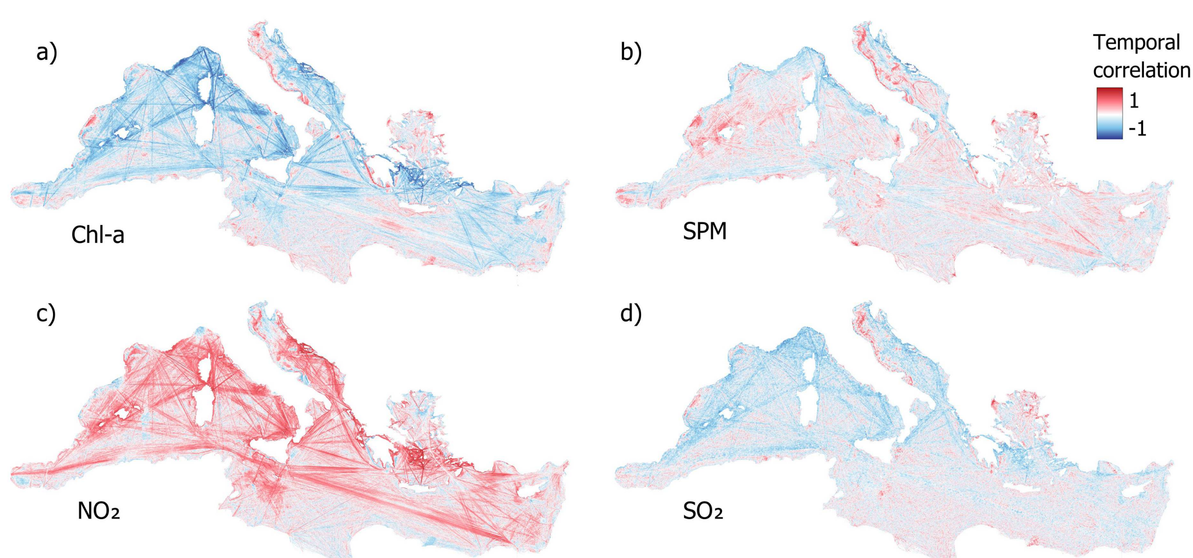

Figure 14. Pixel-level temporal correlation between vessel route density and water quality indicators across the Mediterranean Sea: (a) Chl-a, (b) SPM, (c) NO_2, (d) SO_2.

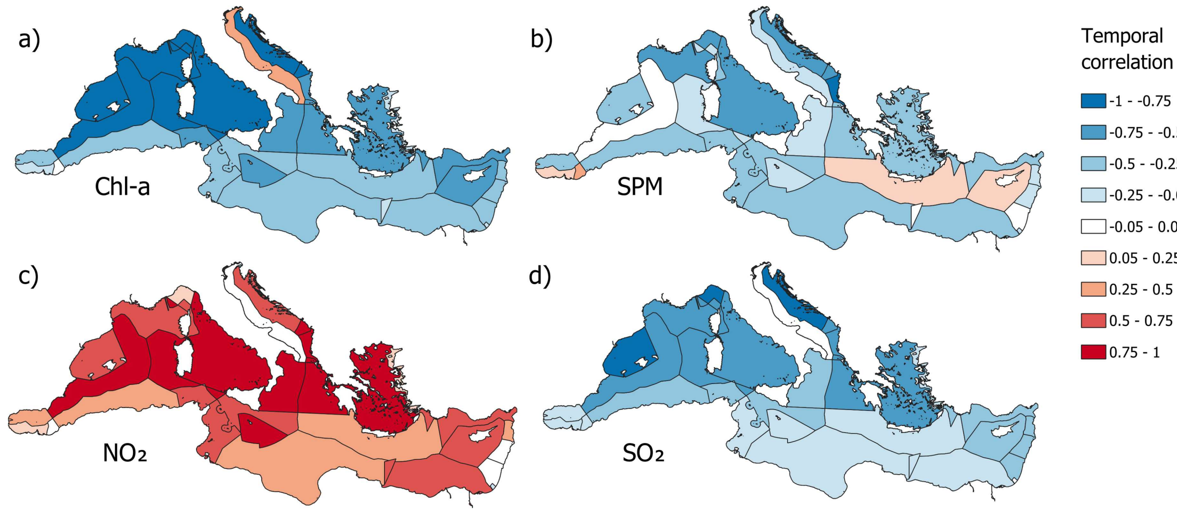

Figure 15. Regional-level temporal correlation between vessel route density and water quality indicators across the Mediterranean sub-basins: (a) Chl-a, (b) SPM, (c) NO_2, (d) SO_2.

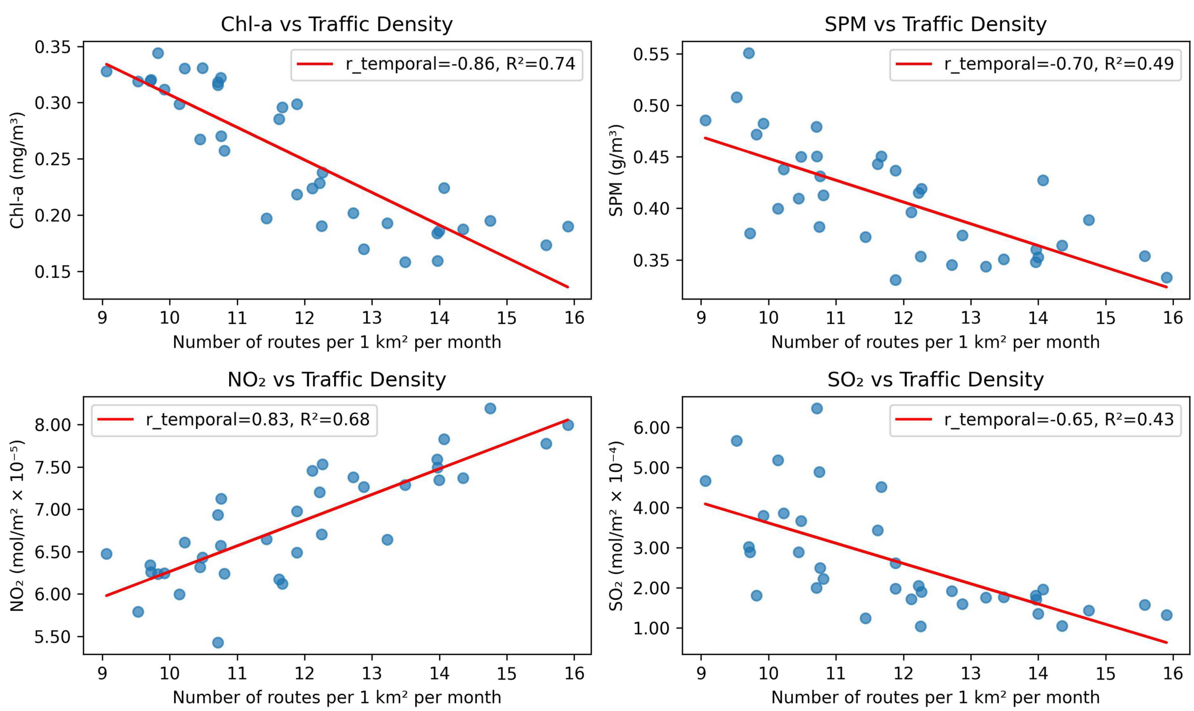

Figure 16. Scatter plots showing basin-wide temporal correlations between vessel route density and water quality indicators across the Mediterranean Sea for the period 2022–2024.

the Albanian and Croatian parts of the Adriatic Sea ($r_{temporal} = -0.76$ and -0.73, respectively, $p < 0.001$), the Italian part of the Tyrrhenian Sea ($r_{temporal} = -0.67$, $p < 0.001$), and weak positive correlations in the Algerian part of the Alboran Sea ($r_{temporal} = 0.44$, $p = 0.007$). SO_2 correlations are predominantly negative, especially in the Spanish part of the Balearic (Iberian) Sea ($r_{temporal} = -0.80$, $p < 0.001$) and the Croatian part of the Adriatic Sea ($r_{temporal} = -0.79$, $p < 0.001$).

Differences between pixel-level and regional correlations reflect the effect of spatial aggregation. At the pixel level, correlations capture localized interactions between shipping activity and environmental variables, often revealing clear patterns along major maritime routes. However, when values are averaged within larger subregions, local signals become mixed due to strong spatial heterogeneity of the indicators.

Environmental variables often vary substantially within regional boundaries, and spatial averaging smooths these differences. In addition, localized extreme values may disproportionately influence the regional mean. As a result, regional correlations may weaken or even change sign compared with pixel-level estimates. This effect is particularly evident for water quality indicators, such as SPM.

In contrast, atmospheric NO_2 maintains a consistently positive correlation with shipping density across spatial scales due to its direct origin from ship exhaust emissions and its relatively short atmospheric lifetime. Because NO_2 concentrations are closely linked to emission sources along shipping routes, this relationship remains detectable even after spatial aggregation of the data.

At the basin-wide level (Figure 16), a strong positive temporal correlation is observed only for NO_2 ($r_{temporal} = 0.83$, $p < 0.001$). In contrast, all other indicators exhibit negative correlations with traffic density, including Chl-a ($r_{temporal} = -0.86$, $p < 0.001$), SPM ($r_{temporal} = -0.70$, $p < 0.001$) and SO_2 ($r_{temporal} = -0.65$, $p < 0.001$). This suggests that, on average, across the Mediterranean Sea, periods of intensified maritime traffic coincide with increases in atmospheric NO_2 concentrations but declines in major water quality indicators such as Chl-a, SPM, and SO_2.

Figure 17 further details the basin-wide temporal correlation coefficients between maritime traffic density and environmental indicators across different vessel types. Distinct association patterns are evident depending on vessel category and pollutant.

All vessel types show a negative correlation with Chl-a, implying that higher maritime activity is generally associated with reduced phytoplankton biomass, possibly due to increased water turbulence, shading or contamination near shipping routes. The strongest negative relationships are observed for passengers ($r_{temporal} = -0.95$ and p value <0.001) and other vessels ($r_{temporal} = -0.90$, $p < 0.001$), suggesting that months with intensified coastal and short-range traffic coincide with reduced basin-wide chlorophyll-a levels. This pattern may reflect enhanced physical disturbance (e.g. mixing, wake-induced turbulence), increased turbidity or cumulative anthropogenic pressure in heavily navigated zones. The consistency of the negative sign across vessel types strengthens the robustness of this association at the basin scale.

For SPM, relationships are weaker and more heterogeneous. Cargo ($r_{temporal} = -0.23$, $p = 0.17$) and tanker ($r_{temporal} = 0.28$, $p = 0.09$) traffic show weak and statistically insignificant correlations, whereas passenger ($r_{temporal} = -0.78$, $p < 0.001$) and other vessels ($r_{temporal} = -0.72$, $p < 0.001$) display stronger negative associations. This suggests that basin-wide SPM dynamics are influenced not only by traffic but also by hydrodynamic processes, river discharge and seasonal variability, which may mask or modulate shipping-related effects.

In contrast, correlations with NO_2 are consistently positive for all vessel types, highlighting the direct contribution of maritime operations to local nitrogen dioxide emissions. The highest coefficients occur for

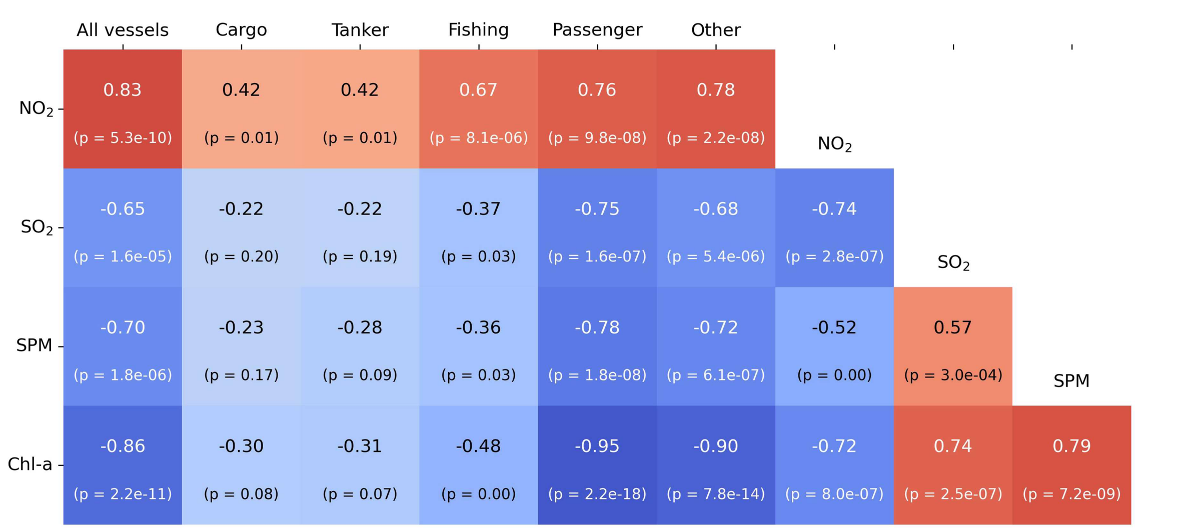

Figure 17. Correlation heatmap showing basin-wide temporal relationships among maritime route density and water quality indicators for different vessel types.

'other' ($r_{temporal} = 0.78$, $p < 0.001$), passenger ($r_{temporal} = 0.76$, $p < 0.001$) and fishing ($r_{temporal} = 0.67$, $p < 0.001$) vessels, confirming that both smaller vessels and passenger traffic play a notable role in air quality degradation.

SO_2 correlations are predominantly negative and generally weaker than those for NO_2. This pattern is somewhat counterintuitive, as higher shipping intensity would normally be expected to increase sulfur emissions. One possible explanation is the implementation of stricter sulfur limits in marine fuels introduced by the International Maritime Organization in 2020, which substantially reduced SO_2 emissions per vessel. As a result, traffic intensity along major routes may remain stable or increase while sulfur emissions may decline due to cleaner fuels and improved engine technologies. Consequently, the observed negative correlations may reflect the influence of regulatory and technological changes rather than a direct proportional relationship between traffic volume and sulfur emissions.

Overall, the results indicate that the strength and direction of the traffic–environment relationship vary by vessel type and pollutant. Passenger and smaller vessels show the strongest temporal associations, while cargo and tanker ships exhibit weaker correlations, likely reflecting differences in routing and operational patterns. However, these relationships should be interpreted cautiously. Part of the observed coupling may arise from shared seasonal dynamics: many environmental indicators follow strong seasonal cycles driven by natural oceanographic and atmospheric processes, whereas maritime traffic, especially passenger traffic, peaks in summer and declines in winter. This seasonal contrast can amplify basin-scale temporal correlations.

Spatial correlation between maritime traffic and water quality indicators

In contrast to temporal correlation, which evaluates how changes in maritime traffic and water quality indicators covary over time at each location, spatial correlation analysis assesses how strongly these variables are related across the study area at a given moment in time. In our case, it quantifies the overall spatial dependence between vessel route density and water quality indicators within the Mediterranean Sea.

At the pixel level (Table 3), spatial correlations between vessel route density and water quality indicators are generally low in magnitude; however, they remain statistically significant ($p < 0.001$), which should be interpreted with caution due to the large sample size.

Among all indicators, NO_2 exhibits the strongest and most consistent positive correlation with traffic density ($r_{spatial} = 0.23$ for all vessels, $p < 0.001$), reflecting the spatial overlap between areas of intense navigation and zones of increased atmospheric nitrogen dioxide concentrations.

For Chl-a, a marginal positive correlation is observed ($r_{spatial} = 0.06$, $p < 0.001$), while SPM and SO_2 display near-zero spatial correlations ($r_{spatial} = 0.03$ and 0.05, $p < 0.001$, respectively). The low magnitude of these spatial correlations reflects the highly localized nature of maritime traffic: shipping primarily occurs along narrow transport corridors that occupy only a small fraction of the total pixels in the Mediterranean. When correlations are computed across the entire basin, most pixels experience little or no traffic but still

Table 3. Pixel-level spatial correlations between maritime route density and water quality indicators for different vessel types.

	Water quality indicator			
Vessel type	Chl-a	SPM	NO_2	SO_2
Cargo	0.01 *(p = 0.03)*	−0.01 *(p < 0.001)*	0.21 *(p < 0.001)*	0.04 *(p < 0.001)*
Tanker	0.006 *(p = 0.04)*	−0.02 *(p < 0.001)*	0.19 *(p = 0)*	0.04 *(p = 0.01)*
Fishing	0.10 *(p < 0.001)*	0.13 *(p < 0.001)*	0.15 *(p < 0.001)*	0.04 *(p < 0.001)*
Passenger	0.02 *(p < 0.001)*	0.00 *(p = 0.11)*	0.08 *(p < 0.001)*	0.02 *(p = 0.025)*
Other	0.04 *(p < 0.001)*	0.02 *(p = 0.027)*	0.11 *(p < 0.001)*	0.02 *(p = 0.007)*
All vessels	0.06 *(p < 0.001)*	0.03 *(p < 0.001)*	0.23 *(p < 0.001)*	0.05 *(p < 0.001)*

display substantial natural variability in environmental indicators (e.g. Chl-a, SPM, ADG), which dilutes the shipping signal and results in weak correlations.

When the correlation is calculated using monthly values of route density and indicators averaged over EEZ-IHO regions, rather than pixel values, stronger relationships emerge (Table 4).

For all vessels combined, spatial correlation coefficients reach 0.27 ($p = 0.13$) for Chl-a and 0.49 for NO_2 ($p = 0.004$), indicating that regional patterns of maritime activity are more closely aligned with the spatial distribution of these indicators than at the pixel level. However, only the correlation for NO_2 is statistically significant, while the correlation for Chl-a should be interpreted with caution. This likely reflects the influence of geographically persistent factors, such as port activity, shipping lanes and regional emission regimes.

Cargo and tanker traffic show particularly strong spatial correlations with NO_2 ($r_{spatial} = 0.50$, $p = 0.003$ and $r_{spatial} = 0.41$, $p = 0.02$, respectively), consistent with their dominant contribution to maritime emissions. In contrast, correlations for fishing vessels with SPM are moderate ($r_{spatial} = 0.37$, $p = 0.16$) but not statistically significant, possibly reflecting localized sediment resuspension near coasts and harbors where these vessel types are most active.

Overall, the spatial correlation analysis indicates that the intensity of maritime activity is most strongly and consistently associated with atmospheric NO_2 concentrations, while its spatial relationship with water-based indicators, such as Chl-a and SPM, varies regionally and is weaker at finer spatial resolutions.

Kruskal–Wallis analysis of traffic-class effects on Chl-a and ADG

The Kruskal‑Wallis H test showed that Chl-a concentrations and ADG values differed significantly among the three maritime vessel route density classes (low, medium and high) for every analyzed year ($p < 0.001$). The distributions for each indicator across classes are presented in Figure 18. The mean ranks for both indicators were consistently highest in the high-traffic class and lowest in the low-traffic class, indicating systematic differences in the distribution of values between intensity groups.

Descriptive statistics for both indicators are summarized in Table 5. All the coefficients of variation (CV %) exceed 35%, indicating substantial internal variability within each traffic class. This wide spread, also visible in the boxplots (Figure 18), reflects the natural spatial heterogeneity of the Mediterranean basin, where coastal upwelling zones, river plumes and oligotrophic open-sea regions may occur within the same traffic class. The medium-traffic class shows the lowest variability for both Chl-a (CV = 151.2%) and ADG (CV = 70.2%), suggesting slightly more homogeneous environmental conditions at intermediate traffic levels.

Despite this high within-class variability, the distributions remain systematically different across traffic classes. Median Chl-a values were higher in the high-traffic class across all years, while the low-traffic class showed lower medians and greater spread (Figure 18a). ADG exhibited a similar pattern, with significantly higher ranked values in the high-traffic class compared to Medium and low-traffic classes (Figure 18b).

The H statistics decreased slightly from 2022 to 2024, suggesting that the contrast between classes weakened modestly over time, although all differences remained highly significant due to the large sample size (Tables 6 and 7).

Table 4. Regional-scale spatial correlations between maritime route density and water quality indicators for different vessel types.

	Water quality indicator			
Vessel type	Chl-a	SPM	NO_2	SO_2
Cargo	0.21 *(p = 0.24)*	−0.001 *(p = 0.64)*	0.50 *(p = 0.003)*	0.10 *(p = 0.53)*
Tanker	0.16 *(p = 0.39)*	−0.06 *(p = 0.71)*	0.41 *(p = 0.02)*	0.07 *(p = 0.52)*
Fishing	0.35 *(p = 0.13)*	0.37 *(p = 0.16)*	0.30 *(p = 0.09)*	0.10 *(p = 0.39)*
Passenger	0.19 *(p = 0.23)*	0.04 *(p = 0.73)*	0.09 *(p = 0.45)*	0.06 *(p = 0.37)*
Other	0.20 *(p = 0.24)*	0.01 *(p = 0.67)*	0.44 *(p = 0.02)*	0.13 *(p = 0.4)*
All vessels	0.27 *(p = 0.13)*	0.03 *(p = 0.64)*	0.49 *(p = 0.004)*	0.11 *(p = 0.45)*

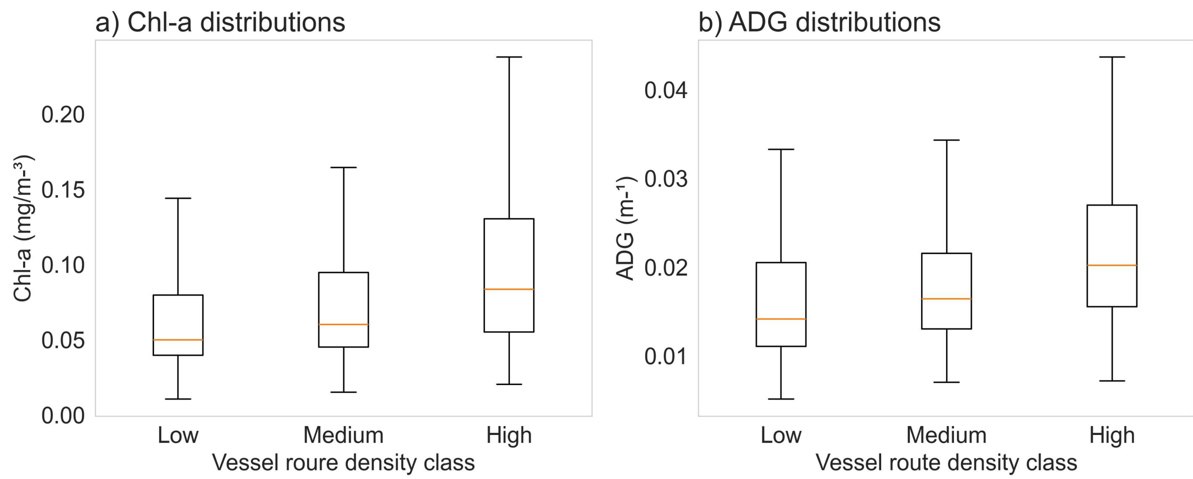

Figure 18. Distribution of Chl-a (a) and ADG (b) concentrations across low-, medium- and high-traffic classes for 2022–2024.

Table 5. Descriptive statistics of Chl-a and ADG across maritime traffic intensity classes (2022–2024).

Traffic class	n	Mean	SD	Min	Max	CV%
Chl-a (mg/m^3)						
Low	3,281,300	0.124	0.346	0.005	6.679	278.1
Medium	3,187,571	0.091	0.138	0.013	6.666	151.2
High	3,219,528	0.145	0.250	0.014	6.574	172.7
ADG (m^{-1})						
Low	3,281,300	0.023	0.031	0.003	0.418	139.6
Medium	3,187,571	0.019	0.014	0.003	0.417	70.2
High	3,219,528	0.025	0.021	0.004	0.418	82.6

Table 6. Summary of Kruskal–Wallis test results for Chl-a concentration across maritime traffic intensity classes (2022–2024).

Year	H statistic	p value	Significance ($p^{abj} < 0.05$)	N	Interpretation
2022	180,142	<0.001	Yes	1,938,214	Strong differences between traffic classes
2023	147,477	<0.001	Yes	1,938,763	Slightly weaker differences
2024	128,183	<0.001	Yes	1,939,761	Still significant contrast further reduced

Since the global Kruskal-Wallis tests were significant for all indicators and years, Dunn's post-hoc tests with Holm correction were applied to identify which traffic-intensity classes differed from each other. All pairwise comparisons (low-medium, low-high and medium-high) remained statistically significant after correction (adjusted $p < 0.05$), confirming that each class represents a distinct distribution of Chl-a and ADG values.

Overall, the results indicate that maritime traffic intensity is associated with consistent and statistically significant differences in both the Chl-a concentration and ADG across the Mediterranean for the entire 2022–2024 period, although the contrast between traffic classes shows a slight decline over time.

Relationship between maritime traffic intensity and heavy metal concentrations

Table 8 summarizes the Pearson correlation coefficients between maritime traffic intensity and heavy metal concentrations (Cd, Pb, Hg and Ni) across different buffer sizes (500 m–10 km) and sample media (water, sediment and biota). Figure 19 illustrates the corresponding regional spatial patterns.

Overall, the relationships are generally weak to moderate, varying by element, medium and spatial scale. Correlations tend to stabilize and often strengthen as the buffer size increases from 0.5 km to 10 km, indicating that the influence of shipping activity becomes more evident at broader spatial scales corresponding to the main navigation corridors.

Table 7. Summary of Kruskal–Wallis test results for ADG values across maritime traffic intensity classes (2022–2024).

Year	*H* statistic	*p* value	Significance ($p^{abj} < 0.05$)	*N*	Interpretation
2022	180,174	<0.001	Yes	1,938,214	Strong differences between traffic classes
2023	133,048	<0.001	Yes	1,938,763	Weaken differences
2024	125,253	<0.001	Yes	1,939,761	High- vs low-traffic contrast reduced

Table 8. Pearson correlation coefficients (*r*) between maritime traffic intensity and heavy metal concentrations (Cd, Pb, Hg and Ni) across different spatial buffers (500 m, 1 km, 5 km and 10 km) and sample media (water, sediment and biota).

Metal\buffer		500 m	1 km	5 km	10 km
Cadmium	Water	−0.06 (*p* = 0.42)	−0.06 (*p* = 0.332)	0.02 (*p* = 0.797)	0.04 (*p* = 0.516)
	Sediment	−0.03 (*p* = 0.471)	−0.03 (*p* = 0.407)	−0.01 (*p* = 0.727)	−0.04 (*p* = 0.312)
	Biota	−0.12 (*p* = 0.475)	−0.13 (*p* = 0.390)	−0.16 (*p* = 0.282)	−0.08 (*p* = 0.595)
	Total	−0.03 (*p* = 0.428)	−0.03 (*p* = 0.363)	−0.01 (*p* = 0.656)	−0.03 (*p* = 0.340)
Lead	Water	0.06 (*p* = 0.423)	0.12 (*p* = 0.043)	0.13 (*p* = 0.028)	0.11 (*p* = 0.081)
	Sediment	0.10 (*p* = 0.008)	0.14 (*p* < 0.001)	0.21 (*p* < 0.001)	0.20 (*p* < 0.001)
	Biota	0.52 (*p* < 0.001)	0.40 (*p* = 0.005)	0.52 (*p* < 0.001)	0.53 (*p* < 0.001)
	Total	0.10 (*p* = 0.003)	0.13 (*p* < 0.001)	0.20 (*p* < 0.001)	0.21 (*p* < 0.001)
Mercury	Water	0.06 (*p* = 0.388)	0.07 (*p* = 0.245)	0.09 (*p* = 0.152)	0.09 (*p* = 0.167)
	Sediment	−0.05 (*p* = 0.279)	−0.05 (*p* = 0.241)	−0.07 (*p* = 0.091)	−0.10 (*p* = 0.016)
	Biota	−0.19 (*p* = 0.098)	−0.20 (*p* = 0.064)	−0.27 (*p* = 0.009)	−0.25 (*p* = 0.015)
	Total	−0.04 (*p* = 0.291)	−0.04 (*p* = 0.217)	−0.06 (*p* = 0.064)	−0.08 (*p* = 0.017)
Nickel	Water	0.19 (*p* = 0.006)	0.26 (*p* < 0.001)	0.25 (*p* < 0.001)	0.22 (*p* < 0.001)
	Sediment	−0.02 (*p* = 0.58)	−0.02 (*p* = 0.515)	−0.03 (*p* = 0.35)	−0.03 (*p* = 0.467)
	Biota	−0.18 (*p* = 0.355)	−0.13 (*p* = 0.457)	−0.19 (*p* = 0.262)	−0.23 (*p* = 0.168)
	Total	−0.02 (*p* = 0.575)	−0.02 (*p* = 0.519)	−0.03 (*p* = 0.351)	−0.02 (*p* = 0.516)

Among the examined metals, lead (Pb) shows the most consistent and robust positive association with maritime traffic, particularly in sediment ($r = 0.14$–0.21, $p < 0.001$) and biota ($r = 0.40$–0.53, $p < 0.005$). Regionally (Figure 19), positive correlation dominates the Western–Central Mediterranean (Ligurian–Tyrrhenian–Ionian) and parts of the Aegean; negative/weak values appear locally in embayments and areas with sparse observations. Lead shows a robust positive traffic signal that strengthens at larger spatial scales and in sediment/biota.

For nickel (Ni) at the whole-basin scale, water exhibits a relatively higher, though still weak positive correlation with vessel route density ($r = 0.19$–0.26, $p < 0.006$ for 0.5–10 km buffers), while sediment and biota are weaker and less consistent. Regional maps (Figure 19) confirm a mosaic pattern: positive correlation in several eastern/southern sectors and weakly negative in parts of the Adriatic/Aegean. Cadmium (Cd) and mercury (Hg) display largely weak or inconsistent relationships with traffic. Cd correlations are near zero overall, with isolated positive values in southern sediments. Hg shows predominantly negative correlations, particularly in biota, consistent with its complex biogeochemistry and multiple non-shipping sources.

Across all the metals, sediment generally shows stronger correlations than does water or biota, suggesting that mechanical disturbance and resuspension from vessel movement contribute to metal redistribution near busy maritime corridors. Lead and, to a lesser extent, nickel thus emerge as the most responsive to maritime traffic intensity at the basin scale.

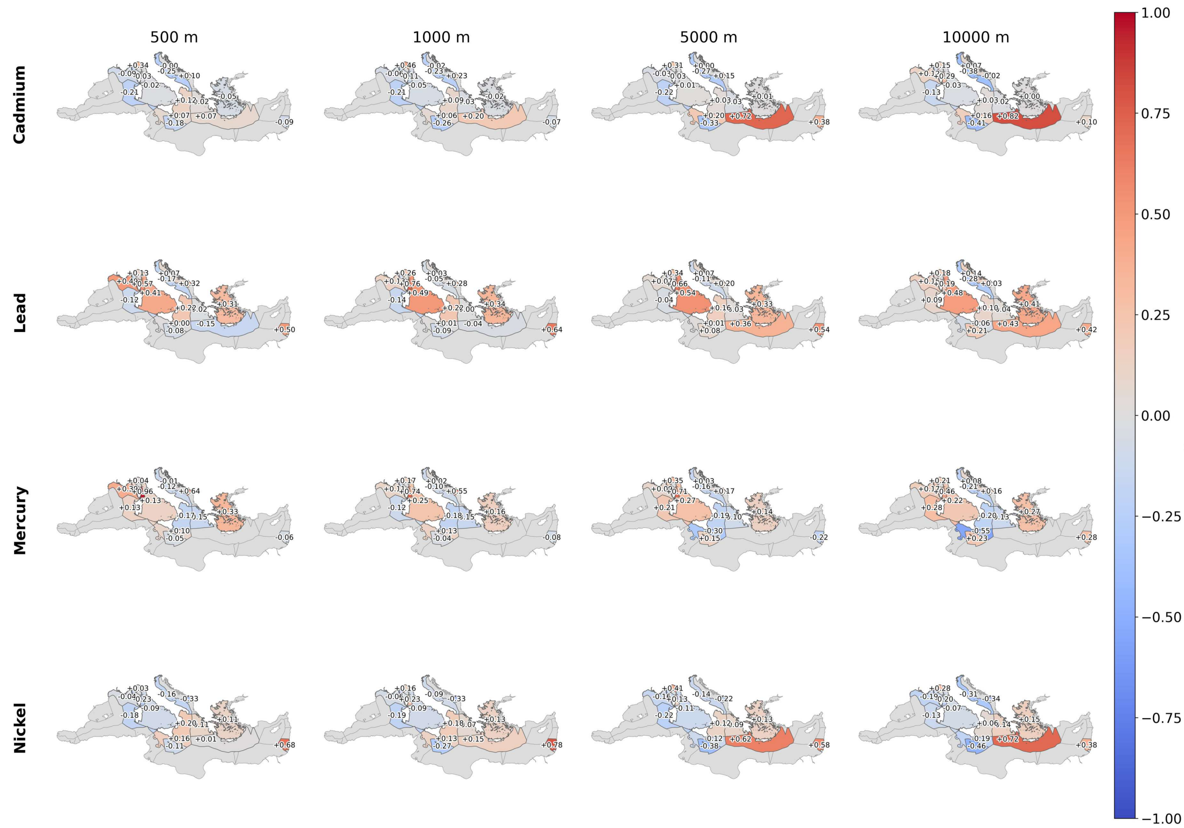

Figure 19. Correlation between maritime route density and heavy metal concentrations across EEZ-IHO regions for different spatial buffers (500 m, 1 km, 5 km and 10 km).

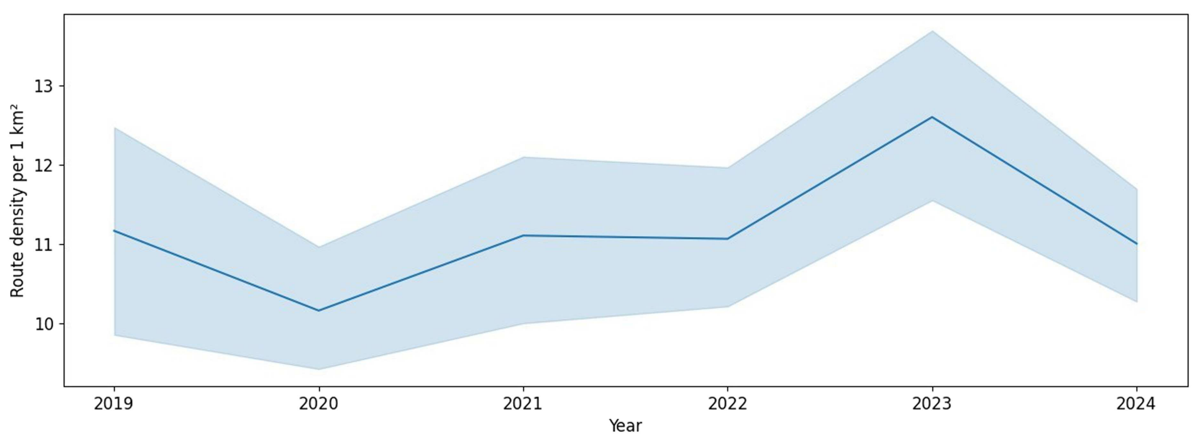

Figure 20. Monthly averages of maritime route density across the Mediterranean Sea, 2019–2024.

Temporal trends and relationships between annual growth rates of maritime traffic and environmental indicators

Figure 20 presents the mean monthly vessel route density averaged across the Mediterranean Sea during 2019–2024. Although the core analysis in this study focuses on the 2022–2024 period, here, we included pre- and mid-pandemic years (2019–2021) to assess whether the COVID-19 lockdowns had a measurable impact on maritime traffic intensity.

The graph reveals a marked decrease in route density in 2020, coinciding with the peak of the pandemic and global transport restrictions. However, vessel activity return to normal in 2021, reaching levels comparable to 2019. A sharp increase is observed in 2023, followed by a moderate decline in 2024, returning to approximately postpandemic conditions. Therefore, maritime traffic during 2022–2024 can be considered broadly representative of typical, postrecovery (near pre-COVID-19) conditions.

Figure 21 illustrates the basin-wide monthly averages of vessel route density and water quality indicators (NO_2, SO_2, TSS and Chl-a) for 2022–2024. The seasonal dynamics show a clear coupling between maritime activity and atmospheric composition: peaks in route density (May–June) coincide with increased NO_2 concentrations and pronounced decreases in Chl-a and SO_2, while traffic minima (October–February) correspond to lower NO_2 and higher values of the other indicators. This pattern suggests that variations in maritime emissions strongly influence atmospheric NO_2, while the response of aquatic indicators, such as Chl-a and SPM, is more complex.

To further explore these dynamics, we analyzed the annual growth rate (AGR) of both maritime traffic and environmental indicators for 2022–2024. Figure 22 presents the AGR of route density at the pixel and regional levels, whereas Figures 23 and 24 depict the AGR of water quality indicators on the same scales.

According to Figure 22a, a substantial decrease in route density occurred along the main corridor from Tanger-Med (Port of Tanger Med, Morocco, MAPTM) to As Suways (Port of Suez, Egypt, EGSUZ), spanning the central Mediterranean from the western African coast through Italy toward the Levantine basin, where maritime route density declined by more than 8 routes per pixel on average. In contrast, traffic increased notably in the Aegean and Adriatic Seas and along routes connecting Greece, Malta and southern Italy, with local increases in some areas exceeding +35 route/year per pixel.

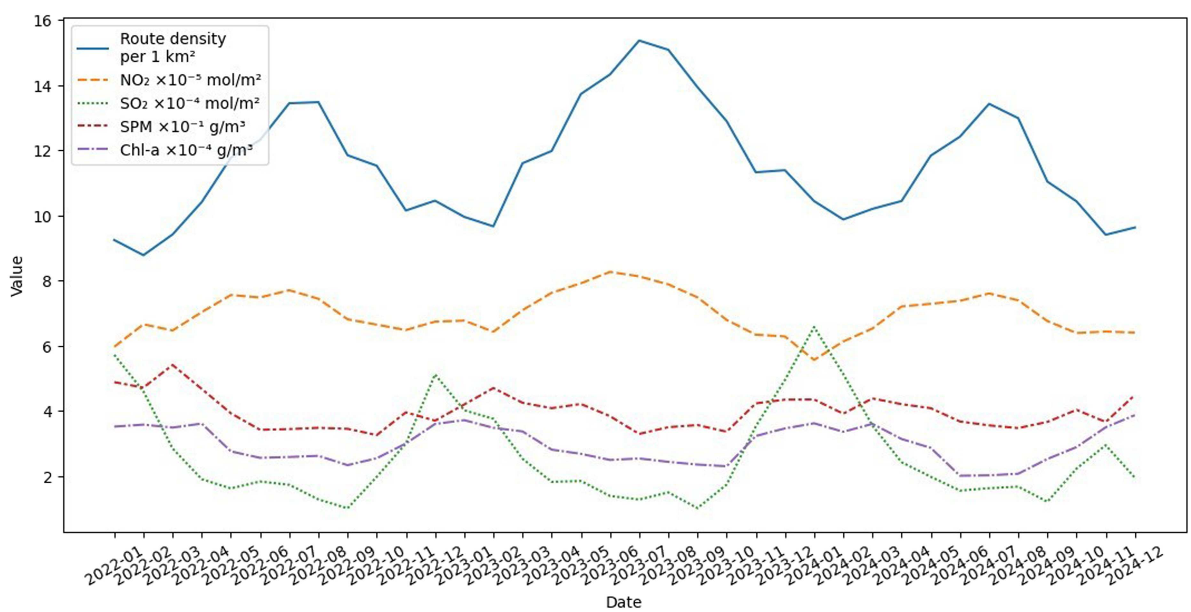

Figure 21. Basin-averaged monthly values of maritime route density and water quality indicators (Chl-a, SPM, NO_2 and SO_2) for 2022–2024.

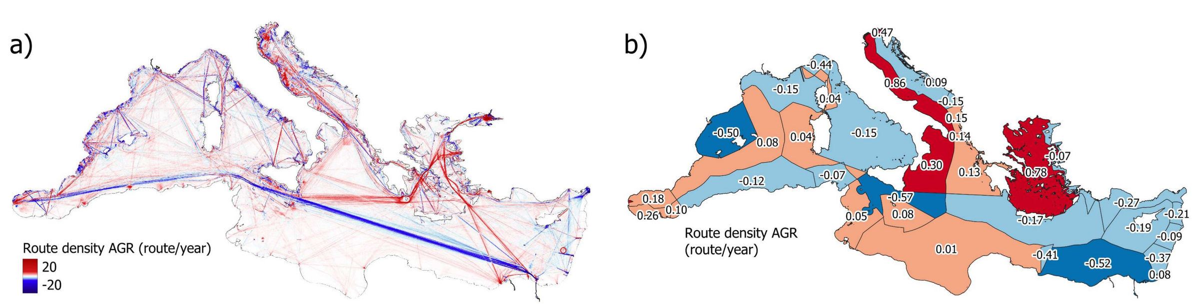

Figure 22. AGR of maritime route density in the Mediterranean Sea during 2022–2024 (routes per year): (a) pixel-level distribution and (b) regional average AGR.

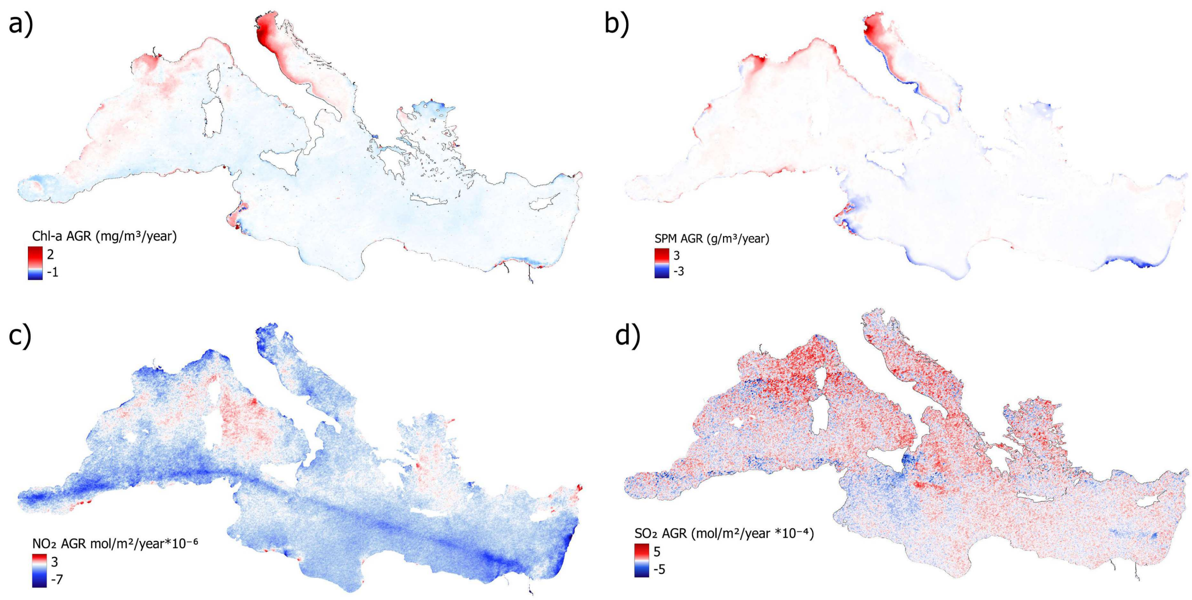

Figure 23. Pixel-level spatial distribution of AGR for water quality indicators during (2022–2024): (a) Chl-a (mg/m^3/year), (b) SPM (g/m^3/year), (c) NO_2 (mol/m^2/year $\cdot 10^{-6}$) and (d) SO_2 (mol/m^2/year $\cdot 10^{-4}$).

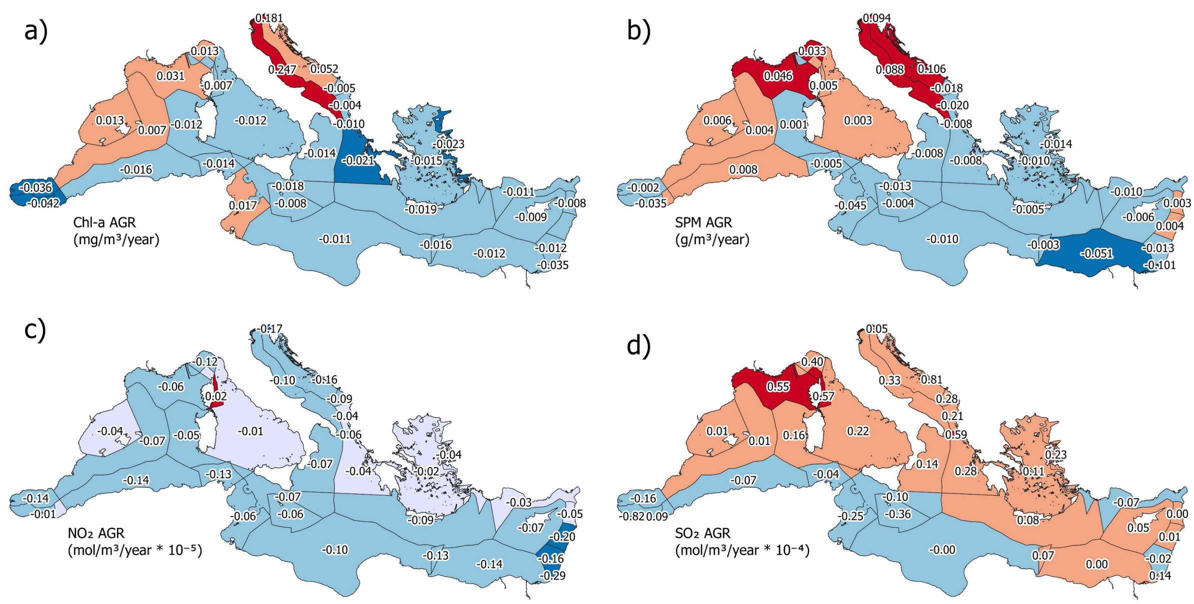

Figure 24. Regional averages of AGR for water quality indicators across the Mediterranean Sea: (a) Chl-a (mg/m^3/year), (b) SPM (g/m^3/year), (c) NO_2 (mol/m^2/year $\cdot 10^{-6}$) and (d) SO_2 (mol/m^2/year^1 $\cdot 10^{-4}$).

The AGR maps of environmental indicators (Figure 23) reveal a corresponding decline in NO_2 concentrations along the same major shipping route where traffic decreased (predominantly around −0.24 mol/m^2/year), confirming a direct emission-related relationship. For other parameters, spatial correspondence is less evident.

Chl-a increased mainly along the Italian Adriatic coast (approximately +2 mg/m^3/year on average) and in the northwestern Mediterranean (near France and Spain, around +0.3 mg/m^3/year) but decreased near the African coastline, mirroring the general decline in SPM in those regions. SO_2 levels, conversely, increased across most of the basin except along the southeastern coast of Sicily and adjacent southern waters, where they slightly declined.

At the regional level (Figure 24), the relationships between traffic and environmental change appear more coherent than at the pixel scale. The highest positive AGR values for Chl-a, SPM and SO_2 are observed in the northern Adriatic, coinciding with areas of intensified maritime activity.

Chl-a generally decreases in high-traffic regions (except in the Adriatic), possibly due to reduced light penetration, vertical mixing and pollutant stress limiting phytoplankton productivity. Meanwhile, moderate increases in Chl-a near the French and Spanish coasts, where traffic has declined, may indicate localized recovery of biological productivity.

SPM patterns are spatially consistent with those of Chl-a, showing similar regional contrasts between northern and southern basins. SO_2 exhibits the weakest spatial associations: slight decreases are observed in central regions despite traffic growth, while increases occur mainly in southern and western sub-basins, particularly near France (+0.55 mol/m^3/year $\cdot 10^{-4}$), where route density declined (−0.50 route/year). This suggests that SO_2 variability may be influenced by additional atmospheric processes, such as long-range transport or nonmarine emission sources.

Table 9 summarizes the correlation coefficients between the regional AGRs of route density and each water quality indicator at different spatial aggregation scales. Correlations increase with region size, indicating that upscaling smooths out local anomalies and noise from small, heterogeneous areas. Several small coastal regions (<50 km^2) exhibited anomalously high or low AGR values—for example, areas with strong traffic decline (−20 route/year) but negligible response in terms of environmental indicators, likely due to their limited spatial representativeness or weak hydrodynamic connectivity. However, even when using regions with an area above 5000 km^2, the correlations remain low, and the associated p values still exceed 0.05, indicating that the observed relationships are not statistically significant at the regional level.

Overall, the spatial analysis results indicate that changes in maritime traffic intensity do not produce a uniform response in water quality indicators across the Mediterranean Sea. These findings suggest that the influence of maritime activity on the marine environment is selective and parameter dependent. Among all indicators, atmospheric NO_2 responds most directly and consistently to traffic variability, while aquatic parameters (Chl-a, SPM, SO_2) exhibit more complex and region-specific responses, reflecting the interplay of physical mixing, biogeochemical processes and local environmental conditions.

Discussion

In this work, we quantified temporal and spatial relationships between maritime traffic intensity and multiple environmental indicators (Chl-a, SPM, ADG, heavy metals, NO_2 and SO_2) across the Mediterranean Sea using multisource data. By analyzing correlations at the pixel, regional and basin-wide levels, we found that these relationships are highly heterogeneous across space and indicator type. Temporal coupling between traffic and NO_2 was strong and consistent, while aquatic indicators (Chl-a, SPM, SO_2) exhibited weaker or region-specific responses, indicating complex interactions between maritime activity and marine environmental conditions, as also reported by Zhu et al. (2024).

The strong positive temporal correlation between maritime traffic and atmospheric NO_2 confirms the dominant role of vessel emissions in shaping nitrogen dioxide variability over the basin. This pattern agrees with previous findings by Fink et al. (2023), Pseftogkas et al. (2024) and El-Zeiny et al. (2025), who also reported elevated NO_2 concentrations along major Mediterranean shipping routes. The observed basin-wide correlation ($r_{\text{temporal}} = 0.83$, $p < 0.001$) suggests that changes in vessel intensity are rapidly

Table 9. Correlation between AGR of route density and water quality indicators calculated for pixels and for regions with different minimum area thresholds (km^2).

Indicator	Pixel level	Area > 0	Area > 100	Area > 1000	Area > 5000
NO_2	0.09	−0.18	−0.11	0.16	0.24
	($p < 0.001$)	*($p = 0.23$)*	*($p = 0.49$)*	*($p = 0.37$)*	*($p = 0.18$)*
SO_2	0.00	−0.12	−0.16	0.09	0.04
	($p < 0.001$)	*($p = 0.41$)*	*($p = 0.32$)*	*($p = 0.59$)*	*($p = 0.81$)*
SPM	−0.00	0.14	0.10	0.18	0.29
	($p < 0.001$)	*($p = 0.34$)*	*($p = 0.54$)*	*($p = 0.29$)*	*($p = 0.11$)*
Chl-a	0.03	0.11	0.14	0.37	0.40
	($p < 0.001$)	*($p = 0.45$)*	*($p = 0.40$)*	*($p = 0.03$)*	*($p = 0.03$)*

reflected in the atmospheric composition, particularly due to direct exhaust emissions from both large cargo ships and smaller coastal fleets. The strongest associations for passenger ($r_{temporal} = 0.76$, $p < 0.001$), fishing ($r_{temporal} = 0.67$, $p < 0.001$) and other ($r_{temporal} = 0.78$, $p < 0.001$) vessels, suggest that these smaller, more maneuverable vessel types, often operating in coastal zones with frequent stops and starts, generate proportionally higher emissions per unit of traffic density compared to larger cargo and tanker ships ($r_{temporal} = 0.42$ each, $p = 0.01$). This could stem from less efficient engine technologies or higher idling times in these categories (Heikkilä & Jalkanen, 2023).

In contrast, the predominantly negative temporal correlations with Chl-a ($r_{temporal} = -0.86$ basin-wide, $p < 0.001$), SPM ($r_{temporal} = -0.70$, $p < 0.001$) and SO_2 ($r_{temporal} = -0.65$, $p < 0.001$) indicate that increased maritime activity may suppress phytoplankton biomass, reduce suspended matter and decouple from sulfur emissions over time. For Chl-a, this inverse relationship may result from the physical disturbance of surface waters and contamination from vessel operations, both of which can reduce light penetration and inhibit photosynthetic activity. Additionally, the seasonal dynamics of Chl-a naturally peak from winter to early spring (Figure 21), whereas maritime traffic intensity is highest in summer. This temporal mismatch likely reinforces the observed negative correlations, as periods of maximum navigation coincide with naturally lower phytoplankton productivity. These effects align with studies by Sarkar et al. (2019), who found that heavy maritime activity can locally reduce primary productivity in enclosed or shallow basins. In addition, the observed relationships appear to be sensitive to the spatial scale of analysis. When data are aggregated to larger regional units, extreme pixel-level values can disproportionately influence regional averages and alter the resulting correlation patterns. Consequently, in the case of temporal correlations, areas where relationships appear predominantly positive or negative at the pixel level may display different patterns after aggregation.

Spatial correlations are weaker than temporal ones, especially at the pixel level ($r_{spatial}$ mostly <0.21, $p < 0.001$), but become stronger when aggregated regionally (e.g. $r_{spatial} = 0.49$, $p = 0.004$ for NO_2 with all vessels, although remain relatively weak for other indicators). This pattern reflects the highly localized nature of maritime traffic: shipping activity is concentrated along narrow transport corridors, whereas a large proportion of pixels across the basin experience little or no traffic. At the same time, environmental indicators may exhibit substantial natural variability even in areas with minimal shipping influence. As a result, when correlations are computed across all pixels, the large number of locations with zero or near-zero traffic dilutes the shipping signal and leads to low spatial correlation values. Regional aggregation partly reduces this noise and allows more persistent relationships associated with dominant shipping corridors to emerge. This scale dependence highlights that the detected correlations partly reflect the statistical properties of spatial averaging and should therefore be interpreted with caution when inferring causal relationships between maritime activity and environmental indicators.

Kruskal–Wallis tests confirmed that Chl-a concentrations and ADG values differed significantly across low-, medium- and high-traffic areas, highlighting the systematic influence of maritime traffic on key water-quality indicators.

Heavy metals exhibited predominantly very low and mostly nonsignificant correlation coefficients ($p > 0.05$) with maritime traffic, varying across elements and environmental media. Lead showed the most consistent positive associations, especially in biota ($r > 0.4$, $p < 0.05$), suggesting a potential influence of resuspension processes and bioaccumulation near shipping routes. In contrast, nickel, cadmium and mercury displayed correlation coefficients close to zero ($p > 0.05$), indicating the likely absence of a direct spatial relationship between these metals and maritime traffic intensity.

AGR analysis (Figures 22–24) shows nonuniform responses: traffic declines in the central corridor reduce NO_2, confirming emission links, but Chl-a and SPM increase in northern areas (e.g. Adriatic) with traffic growth, possibly from enhanced nutrient cycling, and decrease in southern regions. SO_2 shows weak associations, likely due to transboundary transport. AGR correlations strengthen with larger aggregations (Table 9), as upscaling reduces noise from small anomalies like isolated hotspots with extreme traffic changes but limited environmental response.

Overall, maritime traffic's impact is selective: NO_2 responds directly, while Chl-a and SPM show indirect, region-specific effects influenced by ecology, hydrodynamics, and stressors.

Unlike most previous studies that focused on localized ports or coastal areas (Morsy et al., 2022; Muhammed, 2020; Parra et al., 2022; Saliba et al., 2021), our analysis covers the entire Mediterranean basin, integrating both temporal and spatial scales from pixel-level observations to o EEZ-IHO economic subregions and basin-wide aggregates. This approach allowed us to capture cross-basin contrasts between the western and eastern subregions, revealing that traffic–environment interactions are stronger and more consistent in the eastern basin.

By examining the post-COVID-19 period, we provide one of the first basin-scale assessments in the Mediterranean Sea of ‘recovery-era’ maritime emissions and water quality dynamics. The observed rebound in traffic after 2021 and its environmental repercussions reflect a transition toward pre-pandemic conditions. Similar results are reported in studies by Kaamoush et al. (2025) and Athul et al. (2024).

Another novel aspect of this research is the joint evaluation of marine (Chl-a, SPM and heavy metals) and atmospheric (NO_2 and SO_2) indicators. This integrative framework reveals not only direct air–sea coupling (e.g. NO_2-traffic) but also indirect effects on aquatic productivity and suspended matter, bridging previously disconnected research domains.

Nevertheless, some limitations remain. Satellite-based indicators have limited sensitivity near coasts and may be affected by atmospheric correction errors, especially for Chl-a and SPM retrievals. The analysis is also correlative rather than causal; it cannot fully disentangle direct maritime impacts from co-occurring drivers, such as wind forcing, river discharge or regional climate variability. Additionally, heavy metals were assessed only partially due to data availability, restricting deeper interpretation of chemical pollution trends.

Overall, our findings demonstrate that maritime activity continues to exert a measurable influence on Mediterranean environmental conditions, though the strength and direction of this influence depend on both parameter type and region. While air quality indicators respond almost instantaneously to traffic fluctuations, aquatic responses are more complex, governed by regional hydrodynamics and ecological resilience. These insights highlight the importance of integrated, basin-wide monitoring for understanding the multifaceted environmental impacts of shipping.

Conclusions

In this study, we present one of the first basin-wide assessments linking post-COVID-19 shipping recovery during 2022–2024 to atmospheric and water conditions in the Mediterranean Sea. Using harmonized satellite observations and in-situ chemical measurements, we examine multiple indicators (Chl-a, SPM, ADG, NO_2, SO_2 and heavy metals) and quantify their relationships with EMSA-reconstructed vessel-route density data across pixel, EEZ-IHO regional and basin-wide scales.

Overall, temporal correlations were stronger than spatial ones for all investigated indicators, suggesting that environmental responses are more evident in time-series patterns than in spatial gradients.

NO_2 demonstrated a strong and consistent positive correlation with maritime traffic across all analysis levels (e.g. $r_{\text{temporal}} = 0.83$, $p < 0.001$ basin-wide), confirming the direct contribution of ship emissions to atmospheric pollution. In contrast, water-quality indicators displayed weaker and more region-specific responses. Chl-a and SPM generally showed negative correlations with traffic density ($r_{\text{temporal}} < -0.65$, $p < 0.001$ basin-wide), which may partly reflect the inverse seasonal dynamics between maritime traffic and natural ecosystem processes in the Mediterranean, where phytoplankton biomass and suspended matter often increase during cooler months while maritime activity typically peaks in summer. Local hydro-dynamic conditions and coastal inputs may further modulate these relationships. SO_2 also exhibited predominantly negative correlations with traffic intensity, which may reflect the influence of regulatory and technological changes in marine fuels rather than a direct proportional relationship between traffic volume and sulfur emissions.

Vessel-type analysis revealed distinct roles: passenger and fishing vessels exerted the strongest influence on both air and water, due to frequent coastal operations, idling, and wake effects. Cargo and tanker traffic showed weaker, more uniform, reflecting deeper-water routing and lower per-unit emissions.

In addition, Kruskal-Wallis tests indicated that both Chl-a concentrations and ADG values differed significantly among low-, medium- and high-traffic areas throughout 2022-2024, with the highest values observed in high-traffic regions, confirming the systematic influence of traffic intensity on these water-quality indicators.

Heavy-metal analysis revealed weak to moderate spatial associations with vessel density. The most robust positive relationships were observed for Pb in sediments and biota, indicating localized accumulation linked to navigation activity, while Ni, Cd and Hg showed weak correlations, highlighting the influence of additional natural and anthropogenic sources beyond shipping.

AGR analysis showed that traffic reductions along the main trans-Mediterranean corridor (Tangier-Med—Suez) coincided with decreasing NO_2, whereas increasing traffic in the Adriatic coincided with rising Chl-a, SPM and SO_2. However, traffic changes did not produce a uniform environmental response across the basin, and relationships became clearer at coarser aggregation levels, emphasizing the importance of regional-scale assessment.

We detected increasing trends in water-quality degradation in several EEZ-IHO regions, including the Italy, France, Spanish part of the Western Basin and the Adriatic Sea, where traffic intensity and environmental pressures coevolve.

This study demonstrates the value of combining satellite and in-situ monitoring to detect basin-scale environmental patterns, while also highlighting the spatial heterogeneity and indicator-specific nature of shipping impacts. The results support ongoing efforts under the iMERMAID project to improve pollution assessment tools and inform evidence-based marine management and environmental policy in the Mediterranean region.

In future work, we plan to use higher-resolution data, incorporate more in-situ measurements, and conduct similar analyses in other basins such as the Black Sea and Baltic Sea to compare shipping impacts across semi-enclosed seas.

Author contributions

CRediT: **Sofiia Drozd:** Conceptualization, Data curation, Methodology, Software, Validation, Visualization, Writing – original draft, Writing – review & editing; **Pavlo Henitsoi:** Methodology, Validation, Visualization, Writing – original draft, Writing – review & editing; **Miquel Milian Ibáñez:** Validation, Visualization, Writing – original draft, Writing – review & editing; **Julen Guillermo Rostan Saez:** Methodology, Supervision; **Jose Alejandro Donate:** Methodology, Supervision; **Andrii Shelestov:** Funding acquisition, Supervision; **Rodrigo Sedano:** Funding acquisition, Project administration, Supervision; **Nataliia Kussul:** Funding acquisition, Supervision.

Disclosure statement

No potential conflict of interest was reported by the author(s).

Funding

This work was supported by the HORIZON Europe project iMERMAID "Innovative solutions for Mediterranean Ecosystem Remediation via Monitoring and Decontamination from Chemical Pollution" under Grant 101112824.

Data availability statement

The data that support the findings of this study are available from the corresponding author, Sofiia Drozd, upon reasonable request.

References

European Marine Observation and Data Network. (2025). *EMODnet Map Viewer* https://emodnet.ec.europa.eu/geoviewer/

European Marine Observation and Data Network. (2025). *EMODnet product catalogue*. https://emodnet.ec.europa.eu/geonetwork/srv/eng/catalog.search#/metadata/74eef9c6-13fe-4630-b935-f26871c8b661

Ali, M. M., Islam, M. S., Islam, A. R. M. T., Bhuyan, M. S., Ahmed, A. S., Rahman, M. Z., & Rahman, M. M. (2022). Toxic metal pollution and ecological risk assessment in water and sediment at ship breaking sites in the Bay of Bengal coast, Bangladesh. *Marine Pollution Bulletin*, *175*, 113274. https://doi.org/10.1016/j.marpolbul.2021.113274

Ardila, PaR, Álvarez-Alonso, R., Árcega-Cabrera, F., Valsero, J. J. D., García, R. M., Lamas-Cosío, E., Oceguera-Vargas, I., & DelValls, A. (2024). Assessment and review of heavy metals pollution in sediments of the Mediterranean Sea. *Applied Sciences*, *14*(4), 1435. https://doi.org/10.3390/app14041435

Athul, S., Kuttippurath, J., & Patel, V. K. (2024). Changes in global NO_2 pollution by shipping during the COVID-19 lockdown: Implication for sustainable marine operations. *Journal of Hazardous Materials*, *481*, 136482. https://doi.org/10.1016/j.jhazmat.2024.136482

Baghdady, SM, & Abdelsalam, AA (2024). Ten years of oil pollution detection in the Eastern Mediterranean shipping lanes opposite the Egyptian coast using remote sensing techniques. Sci Rep, 14(1), 18057. https://doi.org/10.1038/s41598-024-67983-x

Braga, F., Ciani, D., Colella, S., Organelli, E., Pitarch, J., Brando, V. E., Bresciani, M., Concha, J. A., Giardino, C., Scarpa, G. M., Volpe, G., Rio, M., & Falcini, F. (2022). COVID-19 lockdown effects on a coastal marine environment: Disentangling perception versus reality. *The Science of the Total Environment*, *817*, 153002. https://doi.org/10.1016/j.scitotenv.2022.153002

Calgaro, L., Giubilato, E., Aghito, M., Jalkanen, J., Majamaki, E., Ferrarin, C., Hänninen, R., Palamarchuk, Y., Sofiev, M., Semenzin, E., & Marcomini, A. (2025). Influence of shipping activities on air and water quality in the Northern Adriatic Sea: A high-resolution modelling study. *Marine Pollution Bulletin*, *217*, 118102. https://doi.org/10.1016/j.marpolbul.2025.118102

Chen, X., Dou, S., Song, T., Wu, H., Sun, Y., & Xian, J. (2024). Spatial-temporal ship pollution distribution exploitation and harbor environmental impact analysis via large-scale AIS data. *Journal of Marine Science and Engineering*, *12*(6), 960. https://doi.org/10.3390/jmse12060960

Copernicus Marine Environment Monitoring Service (CMEMS). (2025). *Global ocean colour (Copernicus-GlobColour), Bio-Geo-Chemical, L4 (monthly & interpolated) from Satellite Observations (1997–ongoing)*. Product identifier: OCEANCOLOR_GLO_BGC_L4_MY_009_104. https://doi.org/10.48670/moi-00281

Copernicus Sentinel-5P (processed by ESA). (2018). *TROPOMI Level 2 Nitrogen Dioxide total column products. Version 01. European Space Agency*. https://doi.org/10.5270/S5P-s4ljg54

Drozd, S., Kussul, N., & Shelestov, A. (2025). Improving spatial resolution of aqua MODIS and GCOM-C chlorophyll-a data for Cyprus coastal waters monitoring. *European Journal of Remote Sensing*, *58*(1), 1–21. https://doi.org/10.1080/22797254.2025.2551023

El-Zeiny, A., Nagy, A., & Kaamoush, M. (2025). Impact of maritime and industrial activities on air quality along the Egyptian Mediterranean coast using data observation techniques. *Euro-Mediterranean Journal for Environmental Integration*, *10*, 2883–2896. https://doi.org/10.1007/s41207-025-00803-4

European Marine Observation and Data Network (EMODNET). (2025). *EMODnet Chemistry*. https://emodnet.ec.europa.eu/en/chemistry#contaminants

Fink, L., Karl, M., Matthias, V., Oppo, S., Kranenburg, R., Kuenen, J., Moldanova, J., Jutterström, S., Jalkanen, J., & Majamäki, E. (2023). Potential impact of shipping on air pollution in the Mediterranean region—a multimodel evaluation: Comparison of photooxidants NO_2 and O_3. *Atmospheric Chemistry and Physics*, *23*(3), 1825–1862. https://doi.org/10.5194/acp-23-1825-2023

Flanders Marine Institute.(2024). *The intersect of the Exclusive Economic Zones and IHO sea areas, version 5*. https://doi.org/10.14284/699

Geiger, E. F., Heron, S. F., Hernández, W. J., Caldwell, J. M., Falinski, K., Callender, T., Greene, A. L., Liu, G., De La Cour, J. L., Armstrong, R. A., Donahue, M. J., & Eakin, C. M. (2021). Optimal spatiotemporal scales to aggregate satellite ocean color data for nearshore reefs and tropical coastal waters: Two case studies. *Frontiers in Marine Science*, *8*, 1–14. https://doi.org/10.3389/fmars.2021.643302

Google for Developers. (2025). *GCOM-C/SGLI L3 Chlorophyll-a concentration (V3)*. https://developers.google.com/earth-engine/datasets/catalog/JAXA_GCOM-C_L3_OCEAN_CHLA_V3#citations

GRID-Arendal. (2013). *Maritime transportation routes in the Mediterranean*. https://www.grida.no/resources/5920

He, Y., Jin, S., & Shang, W. (2021). Water quality variability and related factors along the Yangtze river using Landsat-8. *Remote Sensing*, *13*(12), 2241. https://doi.org/10.3390/rs13122241

Heikkilä, M., & Jalkanen, J. (2023). The association between vessel departures and air pollution in Helsinki port area 2016–2021. *Atmosphere*, *14*(4), 757. https://doi.org/10.3390/atmos14040757

Hourany, R. E., Mejia, C., Faour, G., Crépon, M., & Thiria, S. (2021). Evidencing the impact of climate change on the phytoplankton community of the Mediterranean Sea through a bioregionalization approach. *Journal of Geophysical Research Oceans*, *126*(4), 1–20. https://doi.org/10.1029/2020jc016808

Imermaidwebadm. (2025). *iMERMAID*. https://iMERMAID.eu/

Kaamoush, M., El-Sayeh, M., & Omar, M. Y. (2025). Observing air quality in Egypt's Alexandria port based on the consequences of the COVID-19 lockdown. *Discover Sustainability*, *6*(1), 699. https://doi.org/10.1007/s43621-025-01016-z

Kussul, N., Salii, Y., Kuzin, V., Yailymov, B., & Shelestov, A. (2025). Transfer learning and single-polarized Sar image preprocessing for oil spill detection. *ISPRS Open Journal of Photogrammetry and Remote Sensing*, *15*, 100081. https://doi.org/10.1016/j.ophoto.2024.100081

Lacoue-Labarthe, T., Nunes, P. A., Ziveri, P., Cinar, M., Gazeau, F., Hall-Spencer, J. M., Hilmi, N., Moschella, P., Safa, A., Sauzade, D., & Turley, C. (2015). Impacts of ocean acidification in a warming Mediterranean Sea: An overview. *Regional Studies in Marine Science*, *5*, 1–11. https://doi.org/10.1016/j.rsma.2015.12.005

Ledoux, F., Roche, C., Cazier, F., Beaugard, C., & Courcot, D. (2018). Influence of ship emissions on NOx, SO_2, O_3 and PM concentrations in a north-sea harbor in France. *Journal of Environmental Sciences*, *71*, 56–66. https://doi.org/10.1016/j.jes.2018.03.030

Liubartseva, S., Coppini, G., Verdiani, G., Mungari, T., Ronco, F., Pinto, M., Pastore, G., & Lecci, R. (2023). Modeling chronic oil pollution from ships. *Marine Pollution Bulletin*, *195*, 115450. https://doi.org/10.1016/j.marpolbul.2023.115450

Militino, A. F., Ugarte, M. D., & Montesino, M. (2019). Filling missing data and smoothing altered data in satellite imagery with a spatial functional procedure. *Stochastic Environmental Research and Risk Assessment*, *33*(10), 1737–1750. https://doi.org/10.1007/s00477-019-01711-0

Morsy, A., Ebeid, M., Soliman, A., Halim, A. A., Ali, A. E., & Fahmy, M. (2022). Evaluation of the water quality and the eutrophication risk in Mediterranean Sea area: A case study of the port said harbour, Egypt. *Environmental Challenges*, *7*. 100484. https://doi.org/10.1016/j.envc.2022.100484

Muhammed, E. A. (2020). The problem of environmental pollution in the Mediterranean Sea along the coast of Turkey. *Journal of Engineering Studies and Research*, *26*(2), 7–14. https://doi.org/10.29081/jesr.v26i2.161

Mujal-Colilles, A., Guarasa, J. N., Fonollosa, J., Llull, T., & Castells-Sanabra, M. (2022). COVID-19 impact on maritime traffic and corresponding pollutant emissions. The case of the Port of Barcelona. *Journal of Environmental Management*, *310*. 114787. https://doi.org/10.1016/j.jenvman.2022.114787

Murakami, H. (2020). *ATBD of GCOM-C Chlorophyll-a concentration algorithm (Version 2)*. https://suzaku.eorc.jaxa.jp/GCOM_C/data/ATBD/ver2/V2ATBD_O3AB_Chla_Murakami.pdf

Parra, M., Parra, L., Jimenez, J. M., & Lloret, J. (2022). Analysis of the evolution of sea water quality in the spanish coast from satellite images before and during a confinement period. *Journal of Sensors*, *2022*(1), 9996626.

Pseftogkas, A., Koukouli, M., Manders, A., Segers, A., Stavrakou, T., Tokaya, J., Meleti, C., & Balis, D. (2024). Maritime sector contributions on NO_2 surface concentrations in major ports of the Mediterranean basin. *Atmospheric Pollution Research*, *15*(9), 102228. https://doi.org/10.1016/j.apr.2024.102228

Saliba, M., Azzopardi, F., Muscat, R., Grima, M., Smyth, A., Jalkanen, J., Johansson, L., Deidun, A., Gauci, A., Galdies, C., Caruana, T., & Ellul, R. (2021). Trends in vessel atmospheric emissions in the central Mediterranean over the last 10 years and during the COVID-19 outbreak. *Journal of Marine Science and Engineering*, *9*(7), 762. https://doi.org/10.3390/jmse9070762

Sarkar, S. D., Naskar, M., Gogoi, P., Raman, R. K., Manna, R. K., Samanta, S., Mohanty, B. P., & Das, B. K. (2019). Impact assessment of barge trafficking on phytoplankton abundance and Chl a concentration, in river Ganga, India. PLoS One, *14*(9), e0221451. https://doi.org/10.1371/journal.pone.0221451

Schlesinger, W. H. (2021). *Ocean acidification*. Translational Ecology. https://blogs.nicholas.duke.edu/citizenscientist/ocean-acidification/

Selamoglu, M. (2021). The effects of the ports and water transportation on the aquatic ecosystem. *Open Access Journal of Biomedical Science and Research*, *10*(1), 2021.

Shelestov, A., Henitsoi, P., Yailymov, B., & Kussul, N. (2024). Advanced pollutions' monitoring in the Mediterranean Sea: AI-based approach using satellite data and products, *International Conference on Applied Innovations in IT* (Vol. 1338, pp. 605–631). Cham, Springer Nature Switzerland. https://doi.org/10.1007/978-3-031-89296-7_30

Shi, K., & Weng, J. (2021). Impacts of the COVID-19 epidemic on merchant ship activity and pollution emissions in shanghai port waters. *The Science of the Total Environment*, *790*, 148198. https://doi.org/10.1016/j.scitotenv.2021.148198

Soon, Z. Y., Jung, J., Loh, A., Yoon, C., Shin, D., & Kim, M. (2021). Seawater contamination associated with in-water cleaning of ship hulls and the potential risk to the marine environment. *Marine Pollution Bulletin*, *171*, 112694. https://doi.org/10.1016/j.marpolbul.2021.112694

UNEPMAP. (2021). *The blue economy in the Mediterranean*. https://www.unep.org/unepmap/resources/factsheets/blue-economy

Wurtsbaugh, W. A., Paerl, H. W., & Dodds, W. K. (2019). Nutrients, eutrophication and harmful algal blooms along the freshwater to marine continuum. *Wiley Interdisciplinary Reviews Water*, *6*(5), e1373. https://doi.org/10.1002/wat2.1373

Yailymov, B., Kussul, N., Henitsoi, P., & Shelestov, A. (2024). Improving spatial resolution of chlorophyll-a in the Mediterranean Sea based on machine learning. *Radioelectronic and Computer Systems*, *2024*(2), 52–65. https://doi.org/10.32620/reks.2024.2.05

Yan, X., Wang, J., Wu, F., Bai, J., Zhang, X., Li, G., & Fei, H. (2025). Spatial and temporal variation characteristics of air pollutants in coastal areas of China: From satellite perspective. *Remote Sensing*, *17*(11), 1861. https://doi.org/10.3390/rs17111861

Ytreberg, E., Åström, S., & Fridell, E. (2021). Valuating environmental impacts from ship emissions—the marine perspective. *Journal of Environmental Management*, *282*, 111958. https://doi.org/10.1016/j.jenvman.2021.111958

Yuce, A. M., & Altundag, H. (2020). Determination of water quality parameters in Izmit Bay (Marmara Sea) and concentrations of heavy metals by ICP-OES. *Environmental Engineering & Management Journal (EEMJ)*, *19*(12).), 2157–2163 https://www.eemj.eu/index.php/EEMJ/article/view/4240.

Zhang, C., Shi, Z., Zhao, J., Zhang, Y., Yu, Y., Mu, Y., Yao, X., Feng, L., Zhang, F., Chen, Y., Liu, X., Shi, J., & Gao, H. (2021). Impact of air emissions from shipping on marine phytoplankton growth. *The Science of the Total Environment*, *769*, 145488. https://doi.org/10.1016/j.scitotenv.2021.145488

Zhu, W., Li, Y., Jiang, H., Zhang, X., Huang, Y., & Wang, P. (2024). Regionally differentiated responses of chlorophyll-a concentrations to reduced human activity during COVID-19 lockdown in the San Francisco bay area. *Journal of Environmental Management*, *373*, 123801. https://doi.org/10.1016/j.jenvman.2024.123801

Appendix

- ADG—absorption by gelbstoff and detrital material
- AGR—annual growth rate
- AI—artificial intelligence
- Chl-a—chlorophyll-a
- CMEMS—Copernicus Marine Environment Monitoring Service
- DAPSI(W)R(M)—Drivers, Activities, Pressures, State changes, Impact on Welfare, and Responses as Measures
- EEZ—exclusive economic zones
- EMODnet—European Marine Observation and Data Network
- EMSA—European Maritime Safety Agency
- GEE—Google Earth Engine
- IHO—International Hydrographic Organization
- NRTI—near real-time
- SAR—synthetic-aperture radar
- SPM—suspended particulate matter
- STEAM2—Ship Traffic Emission Assessment Model, version 2
- TSS—total suspended solids